Waves in a Cloudy Vortex

DAVID A. SCHECTER

Department of Atmospheric Science, Colorado State University, Fort Collins, Colorado

MICHAEL T. MONTGOMERY

Department of Meteorology, Naval Postgraduate School, Monterey, California, and NOAA/Hurricane Research Division, Miami, Florida

(Manuscript received 26 October 2005, in final form 5 May 2006)

ABSTRACT

This paper derives a system of equations that approximately govern small-amplitude perturbations in a nonprecipitating cloudy vortex. The cloud coverage can be partial or complete. The model is used to examine moist vortex Rossby wave dynamics analytically and computationally. One example shows that clouds can slow the growth of phase-locked counter-propagating vortex Rossby waves in the eyewall of a hurricane-like vortex. Another example shows that clouds can (indirectly) damp discrete vortex Rossby waves that would otherwise grow and excite spiral inertia–gravity wave radiation from a monotonic cyclone at high Rossby number.

1. Introduction

There have been many attempts to understand how wave motions within a tropical cyclone regulate its intensity (see below). Most of these efforts were based on wave theories that neglect moisture. Since clouds pervade tropical cyclones, such an approximation is not soundly justified. The warming or cooling of air parcels by condensation or evaporation of water content can dramatically affect the wave dynamics. In this paper, we will begin to see how.

In particular, we will examine waves in a nonprecipitating cloudy vortex whose basic state has no secondary circulation and is gravitationally stable. In general, the basic state has fluctuations of cloudy and unsaturated air, but those fluctuations are assumed to occur on smaller scales than the waves of interest. We will not consider the effects of boundary layer fluxes, radiative heat fluxes, nor eddy diffusion on the wave dynamics. Furthermore, we will suppose that perturbations are hydrostatic and governed by linearized equations.

In sections 2–5 we will formally develop this model. Although it applies to both hydrostatic inertia–gravity (IG) waves and vortex Rossby (VR) waves, we will focus our attention on the latter.

In section 6, we will briefly reexamine the eyewall instability of a baroclinic cyclone that resembles a category 3 hurricane. Nolan and Montgomery (2002) reported that this particular vortex destabilizes most rapidly by the interaction of counter propagating VR waves on opposite edges of the eyewall. We will show that increased fractional cloud coverage slows the instability, and thereby hinders asymmetric eyewall breakdown. The consequence on hurricane intensity is a topic of ongoing study. On the one hand, potential vorticity mixing after eyewall breakdown can directly reduce the maximum tangential wind speed of a hurricane (e.g., Schubert et al. 1999; Kossin and Schubert 2001). On the other hand, the thermo-fluid dynamics connected to eyewall breakdown is subtle, and may actually lead to a stronger hurricane (Emanuel 1997; Montgomery et al. 2002; Persing and Montgomery 2003; Montgomery et al. 2006).

In section 8, we will examine how moisture influences the discrete VR waves of a barotropic cyclone, whose vertical vorticity decreases monotonically with radius. These waves account for precessing tilts and elliptical (triangular, square, etc.) deformations of the vortex core. If the Rossby number of the cyclone exceeds unity, its baroclinic VR waves can efficiently ex-

Corresponding author address: Dr. David Schecter, NorthWest Research Associates, 14508 NE 20th St., Bellevue, WA 98007.
E-mail: schecter@nwra.com

DOI: 10.1175/JAS3849.1

Report Documentation Page

Form Approved
OMB No. 0704-0188

1. REPORT DATE	2. REPORT TYPE	3. DATES COVERED
MAY 2006		**00-00-2006 to 00-00-2006**

4. TITLE AND SUBTITLE	5a. CONTRACT NUMBER
Waves in a Cloudy Vortex	5b. GRANT NUMBER
	5c. PROGRAM ELEMENT NUMBER
6. AUTHOR(S)	5d. PROJECT NUMBER
	5e. TASK NUMBER
	5f. WORK UNIT NUMBER
7. PERFORMING ORGANIZATION NAME(S) AND ADDRESS(ES) **Naval Postgraduate School,Department of Meteorology,Monterey,CA,93943**	8. PERFORMING ORGANIZATION REPORT NUMBER
9. SPONSORING/MONITORING AGENCY NAME(S) AND ADDRESS(ES)	10. SPONSOR/MONITOR'S ACRONYM(S)
	11. SPONSOR/MONITOR'S REPORT NUMBER(S)

12. DISTRIBUTION/AVAILABILITY STATEMENT
Approved for public release; distribution unlimited

13. SUPPLEMENTARY NOTES

14. ABSTRACT

This paper derives a system of equations that approximately govern small-amplitude perturbations in a nonprecipitating cloudy vortex. The cloud coverage can be partial or complete. The model is used to examine moist vortex Rossby wave dynamics analytically and computationally. One example shows that clouds can slow the growth of phase-locked counter-propagating vortex Rossby waves in the eyewall of a hurricane-like vortex. Another example shows that clouds can (indirectly) damp discrete vortex Rossby waves that would otherwise grow and excite spiral inertia?gravity wave radiation from a monotonic cyclone at high Rossby number.

15. SUBJECT TERMS

16. SECURITY CLASSIFICATION OF:			17. LIMITATION OF ABSTRACT	18. NUMBER OF PAGES	19a. NAME OF RESPONSIBLE PERSON
a. REPORT **unclassified**	b. ABSTRACT **unclassified**	c. THIS PAGE **unclassified**	**Same as Report (SAR)**	**25**	

cite frequency-matched spiral IG waves in the environment (Ford 1994a,b; Polvani et al. 1994; Plougonven and Zeitlin 2002; Schecter and Montgomery 2003, 2004, 2006). Surprisingly, producing IG wave radiation compels a VR wave to grow. Such growth is usually opposed by a critical layer that resonantly absorbs wave activity (Briggs et al. 1970; Pillai and Gould 1994; Schecter et al. 2000, 2002; Balmforth et al. 2001; Mallen et al. 2005). We will show that moisture tends to enhance damping by the critical layer and thereby suppress the radiative instability. Consequently, cloud coverage can inhibit the loss of angular momentum by IG wave radiation. Such loss might otherwise merit some consideration in the angular momentum budget of a hurricane (e.g., Chow and Chan 2003).

The theory of discrete VR waves, especially of the tilt mode, also provides a framework for understanding the response of a vortex to ambient vertical shear. Recent studies (e.g., Jones 1995; Reasor and Montgomery 2001; Schecter et al. 2002; Reasor et al. 2004) have shown that reducing the static stability of the atmosphere typically increases (i) the azimuthal phase velocity and (ii) the decay rate of the discrete tilt mode of a monotonic (or quasi-monotonic) cyclone. Both of these modifications increase the cyclone's natural resistance to misalignment under the influence of ambient shear. As we will show in section 8, increasing the cloud coverage has similar effects on the tilt mode and thereby also improves vortex resilience (cf. Patra 2004). This result is quite reasonable, in light of the aforementioned studies, if one connects denser cloud coverage to lower static stability (e.g., Durran and Klemp 1982).

Another class of VR waves comprises continuum mode disturbances that are sheared by differential rotation of the mean flow. Sheared VR waves that are generated by localized bursts of convection can transport angular momentum toward the radius of maximum wind, and thereby intensify a cyclone (e.g., Montgomery and Kallenbach 1997; Montgomery and Enagonio 1998; Möller and Montgomery 1999, 2000; Enagonio and Montgomery 2001). They may also have some connection to moving spiral rainbands (e.g., Montgomery and Kallenbach 1997). Although we will not directly examine the influence of clouds on sheared VR waves, a theory based on our moist model would be a modest formal extension of the existing dry theory.

On a technical note, the moist wave equations of section 4 are nearly identical to the linearized dry hydrostatic primitive equations. Moisture simply reduces the Eulerian rate of cooling/warming by updrafts/downdrafts by a factor Υ [see Eq. (31)]. The Υ distribution is a property of the basic state of the vortex, and has only radial and vertical variation. Its value indicates the average reduction of the vertical buoyancy restoring force of air parcels along an azimuthal circuit (see appendix G). As the fraction of cloudy air in the circuit increases from zero, Υ decreases from unity. In section 5, we will present a formula for Υ [Eq. (37)] that makes a baroclinic vortex neutral to slantwise convection. In addition, we will examine the spatial distribution of Υ for a realistically simulated hurricane. As expected, we will find that Υ is smallest in the very moist eyewall.

The moist wave equations presented here are an improvement over the usual dry model, and their solutions provide insight into the most basic effects of cloud coverage. Nevertheless, they exclude several factors (see paragraph 2) that might significantly alter wave motions in actual or realistically simulated hurricanes (cf. Wang 2002a,b; Chen and Yau 2001; Chow et al. 2002; Chen et al. 2003; etc.). A more comprehensive theory should be the goal of future research.

The remainder of this paper is organized as follows: section 2 describes our parameterization of moist processes in a cloudy vortex. Section 3 presents the nonlinear hydrostatic fluid equations that are supposed to govern the vortex. Section 4 presents the linearized wave equations. Section 5 discusses some important Υ distributions. Section 6 illustrates how cloud coverage can temper an asymmetric eyewall instability. Section 7 contains a formal discussion of the eigenmode problem for a cloudy vortex. Section 8 examines how cloud coverage can cause or accelerate the decay of discrete VR waves in a monotonic cyclone. Such decay inhibits the radiation of spiral IG waves and improves vortex resilience. Section 9 summarizes our main results. Appendices A–F provide some analytical and computational details for those who may wish to continue the analysis of waves in a cloudy vortex beyond the scope of this paper. Appendix G informally discusses the physical meaning of Υ.

2. Moisture parameterization

a. The water mass equations

Suppose that water has only two phases: vapor (v) and liquid (l). Further suppose that there is no precipitation, and that there is no diffusion of water mass. Then, the total water mixing ratio,

$$q_t \equiv q_v + q_l, \tag{1}$$

is conserved along material trajectories. That is,

$$\frac{dq_t}{dt} = 0. \tag{2}$$

The water vapor mixing ratio is here determined by the diagnostic equation,

$$q_v = \begin{cases} q_t & q_t < q_{v*}, \\ q_{v*} & q_t > q_{v*}, \end{cases} \tag{3}$$

in which $q_{v*}(T, p)$ is the saturation vapor mixing ratio, T is temperature, and p is total pressure.

b. The heat equation

The entropy of a moist fluid parcel, per unit mass of dry air, is given by [e.g., Emanuel 1994, Eq. (4.5.9)]

$$s_m = (c_{pd} + q_t c_l)\ln(T) - R_d \ln(p_d) + L_v q_v / T - q_v R_v \ln(e/e_*). \tag{4}$$

We will assume that

$$\frac{ds_m}{dt} = 0. \tag{5}$$

Above, c_{pd} and c_l are the specific heats of dry air (at constant pressure) and of liquid water; R_d and R_v are the gas constants of dry air and of water vapor; p_d is the pressure of dry air, whereas e and $e^*(T)$ are the actual and saturation values of the water vapor pressure; $L_v(T)$ is the latent heat of vaporization.

We may now derive an equation for the density potential temperature, which is defined by

$$\theta_\rho \equiv \frac{p}{\rho R_d}\left(\frac{p_0}{p}\right)^{R_d/c_{pd}}. \tag{6}$$

Here, ρ is the total mass density of a fluid parcel and p_0 is a reference pressure, taken to be 10^5 Pa.

In the present model, three variables specify the thermodynamic state of a moist air parcel [Eq. (3) eliminates q_v]. We may choose these variables to be p, s_m, and q_t. In terms of these variables, the functional form of θ_ρ differs for saturated (s) and unsaturated (u) air parcels; that is,

$$\theta_\rho = \begin{cases} \theta^u_\rho(p, s_m, q_t) & q_t < q_{v*}, \\ \theta^s_\rho(p, s_m, q_t) & q_t > q_{v*}. \end{cases} \tag{7}$$

For convenience, we introduce the saturation variable

$$\mu \equiv q_t - q_{v*}, \tag{8}$$

which is positive (negative) for saturated (unsaturated) parcels. In addition, let $H(\mu)$ denote the unit step function. Then, we may rewrite Eq. (7) as follows:

$$\theta_\rho = H(-\mu)\theta^u_\rho + H(\mu)\theta^s_\rho. \tag{9}$$

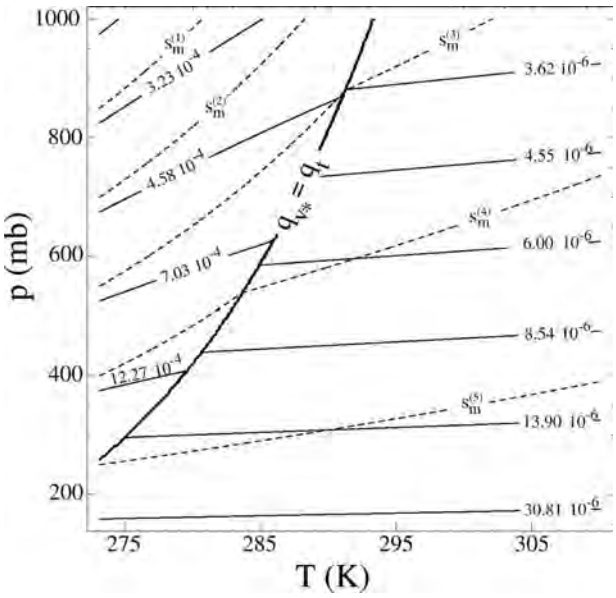

FIG. 1. Contour plot of minus χ for $q_t = 0.015$. The contour labels are in units of K Pa^{-1}. Note that χ is discontinuous across the curve $q_{v*}(T, p) = q_t$, which separates (left) saturated and (right) unsaturated regions. The dashed curves are contours of constant moist entropy $s_m^{(i)}$. The value of entropy increases with the superscript i.

The material derivative of density potential temperature has three terms; specifically,

$$\frac{d\theta_\rho}{dt} = \frac{dp}{dt}\left(\frac{\partial\theta_\rho}{\partial p}\right)_{s_m,q_t} + \frac{ds_m}{dt}\left(\frac{\partial\theta_\rho}{\partial s_m}\right)_{p,q_t} + \frac{dq_t}{dt}\left(\frac{\partial\theta_\rho}{\partial q_t}\right)_{s_m,p}. \tag{10}$$

Inserting Eqs. (2), (5), and (9) into the right-hand side of Eq. (10) yields

$$\frac{d\theta_\rho}{dt} = \frac{dp}{dt}\left[\chi + \delta(\mu)(\theta^u_\rho - \theta^s_\rho)\left(\frac{\partial q_{v*}}{\partial p}\right)_{s_m,q_t}\right], \tag{11}$$

in which

$$\chi \equiv H(-\mu)\left(\frac{\partial\theta^u_\rho}{\partial p}\right)_{s_m,q_t} + H(\mu)\left(\frac{\partial\theta^s_\rho}{\partial p}\right)_{s_m,q_t}. \tag{12}$$

Here, we have used the fact that $dH/d\mu = \delta(\mu)$, in which $\delta(\mu)$ is the Dirac distribution. Figure 1 is a contour plot of minus χ for an air parcel with $q_t = 0.015$. This value of q_t is characteristic of, say, a parcel in the lower region of a tropical storm. Note that the negative value of χ increases by orders of magnitude as a parcel moves from an unsaturated state ($\mu < 0$) to a saturated state ($\mu > 0$) along any path, such as a moist adiabat (dashed curve).

We may simplify Eq. (11) by observing that

$$\theta^u_\rho = \theta^s_\rho \quad \text{if} \quad \mu = 0. \tag{13}$$

Therefore, Eq. (11) reduces to

$$\frac{d\theta_\rho}{dt} = \chi \frac{dp}{dt}, \tag{14}$$

which constitutes our working heat equation. In a dry atmosphere, $\chi = 0$ and θ_ρ is conserved.

In appendix A, we derive the following equations for the thermodynamic derivatives that appear in the definition of χ:

$$\left(\frac{\partial \theta_\rho^u}{\partial p}\right)_{s_m, q_t} = -\frac{TR_d}{pc_{pd}}\left(\frac{p_0}{p}\right)^{R_d/c_{pd}} \frac{1 + q_t/\epsilon}{1 + q_t} \times \left(1 - \frac{1 + q_t/\epsilon}{1 + q_t c_{pv}/c_{pd}}\right) \tag{15}$$

and

$$\left(\frac{\partial \theta_\rho^s}{\partial p}\right)_{s_m, q_t} = -\frac{TR_d}{pc_{pd}}\left(\frac{p_0}{p}\right)^{R_d/c_{pd}} \frac{1 + q_{v*}/\epsilon}{1 + q_t} \left[1 + \frac{c_{pd} q_{v*}}{R_d \epsilon} - \frac{(1 + q_{v*}/\epsilon)\left(1 + \dfrac{q_{v*} L_v}{R_d T}\right)^2}{1 + q_{v*} c_{pv}/c_{pd} + \mu c_l/c_{pd} + \dfrac{L_v^2 q_{v*}(1 + q_{v*}/\epsilon)}{R_v c_{pd} T^2}}\right]. \tag{16}$$

Here, we have introduced the ratio of gas constants $\epsilon \equiv R_d/R_v = 0.622$. Since $q_{v*} = q_{v*}(T, p)$ and $L_v = L_v(T)$, the right-hand sides of Eqs. (15) and (16) are functions of the measurable quantities T, p, and q_t.

3. The moist primitive equations

For the remainder of this paper, we will assume that vertical accelerations are small and that hydrostatic balance applies. Consequently, we may use p as the vertical coordinate instead of height. In addition, we will assume that the vortex occupies a sufficiently small section of the globe where the f-plane approximation is valid.

In pressure coordinates, the horizontal velocity equation takes the form

$$\left(\frac{\partial}{\partial t} + \mathbf{u} \cdot \boldsymbol{\nabla}_p\right)\mathbf{u} + \omega \frac{\partial \mathbf{u}}{\partial p} = -\boldsymbol{\nabla}_p \phi + \mathbf{u} \times f\hat{\mathbf{z}}, \tag{17}$$

in which $\mathbf{u}$ is the horizontal velocity vector, $\omega \equiv dp/dt$, f is the constant Coriolis parameter, and $\phi = gz$ is the geopotential. Furthermore, $\hat{\mathbf{z}}$ is the vertical unit vector, and $\boldsymbol{\nabla}_p$ is the horizontal gradient operator, with spatial derivatives evaluated at constant p.

The heat equation (14) and conservation of water mass (2) take the forms

$$\left(\frac{\partial}{\partial t} + \mathbf{u} \cdot \boldsymbol{\nabla}_p\right)\theta_\rho = -\omega\left(\frac{\partial \theta_\rho}{\partial p} - \chi\right) \tag{18}$$

and

$$\left(\frac{\partial}{\partial t} + \mathbf{u} \cdot \boldsymbol{\nabla}_p\right) q_t = -\omega \frac{\partial q_t}{\partial p}, \tag{19}$$

respectively.

In addition to the above prognostic equations, there are two diagnostic equations. Hydrostatic balance yields

$$\frac{\partial \phi}{\partial p} = -\frac{R_d}{p}\left(\frac{p}{p_0}\right)^{R_d/c_{pd}} \theta_\rho, \tag{20}$$

and the mass continuity equation yields

$$\frac{\partial \omega}{\partial p} = -\boldsymbol{\nabla}_p \cdot \mathbf{u}. \tag{21}$$

The auxiliary equation for hydrostatic potential vorticity,

$$\Pi \equiv \boldsymbol{\eta} \cdot \boldsymbol{\nabla} \theta_\rho, \tag{22}$$

is given by

$$\left(\frac{\partial}{\partial t} + \mathbf{u} \cdot \boldsymbol{\nabla}_p\right)\Pi + \omega \frac{\partial \Pi}{\partial p} = \boldsymbol{\nabla} \cdot \omega \chi \boldsymbol{\eta}, \tag{23}$$

in which $\boldsymbol{\nabla} \equiv \boldsymbol{\nabla}_p - \hat{\mathbf{z}}\partial/\partial p$, and

$$\boldsymbol{\eta} \equiv \boldsymbol{\nabla} \times \mathbf{u} + f\hat{\mathbf{z}}. \tag{24}$$

Note that we have used a convention in which the horizontal and vertical components of $\boldsymbol{\nabla}$ have different dimensions (inverse length and inverse pressure). We have used a similar convention for $\boldsymbol{\eta}$. Of course each term of $\boldsymbol{\eta} \cdot \boldsymbol{\nabla}$ (for example) has the same dimension.

4. The wave equations

This section presents a linear model for wave dynamics in a cloudy vortex whose basic state has no secondary circulation. We will use a vortex-centered cylindrical coordinate system in which r and φ are the radius and azimuth, and u and v are the radial and azimuthal velocities. Overbars and primes will mark basic state and perturbation fields, respectively.

a. Balanced basic state

The basic state of an atmospheric vortex is characterized by its azimuthal velocity field $\overline{v}(r, p)$. We may define $\overline{v}$ to be a tempero-azimuthal mean of v. For notational convenience, we introduce the following auxiliary fields:

$$\begin{aligned} &\overline{\Omega}(r,p) \equiv \overline{v}/r, \qquad \overline{\zeta}(r,p) \equiv r^{-1}\partial(r\overline{v})/\partial r \\ &\overline{\eta}(r,p) \equiv \overline{\zeta} + f, \quad \overline{\xi}(r,p) \equiv 2\overline{\Omega} + f. \end{aligned} \tag{25}$$

Here, $\overline{\Omega}$ is the angular rotation frequency, $\overline{\zeta}$ is the relative vertical vorticity, $\overline{\eta}$ is the absolute vertical vorticity, and $\overline{\xi}$ is the modified Coriolis parameter. By assumption, the basic state has no secondary circulation, that is, $\overline{\omega}, \overline{u} = 0$.

The basic-state geopotential $\overline{\phi}(r, p)$ and density potential temperature $\overline{\theta}_\rho(r, p)$ are defined to satisfy gradient balance,

$$\frac{\partial\overline{\phi}}{\partial r} = \frac{\overline{v}^2}{r} + \overline{v}f, \tag{26}$$

and hydrostatic balance,

$$\frac{\partial\overline{\phi}}{\partial p} = -\frac{R_d}{p}\left(\frac{p}{p_0}\right)^{R_d/c_{pd}}\overline{\theta}_\rho. \tag{27}$$

Taking the partial derivative of Eq. (26) with respect to pressure, making use of Eq. (27), and simplifying, we obtain the thermal wind relation,

$$\frac{\partial\overline{\theta}_\rho}{\partial r} = -\frac{p}{R_d}\left(\frac{p_0}{p}\right)^{R_d/c_{pd}}\overline{\xi}\frac{\partial\overline{v}}{\partial p}. \tag{28}$$

The basic state also has a water mass profile $\overline{q}_t(r, p)$, which we take to be a tempero-azimuthal mean of q_t. We further define $\overline{\chi}(r, p)$ to be a tempero-azimuthal mean of χ. Note that the difference between $\overline{\chi}(r, p)$ and $\chi(\overline{\theta}_\rho, \overline{q}_t, p)$ may be substantial if q_t fluctuates between saturated and unsaturated values within the t and φ averaging intervals.

b. Small perturbations

Each field that describes the vortex is, of course, the sum of its basic state and a time-dependent perturbation. Neglecting terms that are quadratic in the perturbation fields, the two components of the horizontal velocity equation (17) may be written

$$\left(\frac{\partial}{\partial t} + \overline{\Omega}\frac{\partial}{\partial\varphi}\right)u' = \overline{\xi}v' - \frac{\partial\phi'}{\partial r} \tag{29}$$

and

$$\left(\frac{\partial}{\partial t} + \overline{\Omega}\frac{\partial}{\partial\varphi}\right)v' = -\overline{\eta}u' - \omega'\frac{\partial\overline{v}}{\partial p} - \frac{1}{r}\frac{\partial\phi'}{\partial\varphi}. \tag{30}$$

Furthermore, the heat equation (18) may be written

$$\left(\frac{\partial}{\partial t} + \overline{\Omega}\frac{\partial}{\partial\varphi}\right)\theta'_\rho = -u'\frac{\partial\overline{\theta}_\rho}{\partial r} - \omega'\Upsilon\frac{\partial\overline{\theta}_\rho}{\partial p}, \tag{31}$$

in which we have introduced the buoyancy reduction factor,

$$\Upsilon(r,p) \equiv \frac{\partial\overline{\theta}_\rho/\partial p - \overline{\chi}}{\partial\overline{\theta}_\rho/\partial p}. \tag{32}$$

Section 5 discusses Υ distributions that might have special relevance to atmospheric vortices. Appendix G explains in detail how Υ measures a local reduction of the vertical buoyancy restoring force that acts on vertically displaced air parcels.

In addition to the above prognostic equations, we have, from hydrostatic balance,

$$\frac{\partial\phi'}{\partial p} = -\frac{R_d}{p}\left(\frac{p}{p_0}\right)^{R_d/c_{pd}}\theta'_\rho, \tag{33}$$

and, from mass continuity,

$$\frac{\partial\omega'}{\partial p} = -\frac{1}{r}\frac{\partial(ru')}{\partial r} - \frac{1}{r}\frac{\partial v'}{\partial\varphi}. \tag{34}$$

We need not consider the linearized equation for total water mass, since the above system (29)–(34) does not depend explicitly on q'_t, and is therefore closed.

Note that the above wave equations are the same as those for a dry vortex, with $\partial\overline{\theta}_\rho/\partial p \to \Upsilon\partial\overline{\theta}_\rho/\partial p$.

Note also that linearization of the heat equation is a bold approximation. Linear theory assumes that quadratic perturbation terms are subdominant to linear terms in the equations of motion. However, $\omega'\chi'$ is not necessarily negligible. Since χ varies discontinuously between unsaturated and cloudy air, χ' can have fluctuations of order $\overline{\chi}$. If these fluctuations have small spatiotemporal scales, they may not appreciably influence the large-scale waves of interest. We defer testing the accuracy of linearization, with high-resolution nonlinear simulations, until a future time.

5. The buoyancy reduction factor

For the remainder of this paper, we will treat the buoyancy reduction factor $\Upsilon(r, p)$ as an adjustable parameter. We will attempt to choose Υ distributions that have some meteorological significance.

a. Υ for symmetric stability

There is a common belief that intense atmospheric vortices, hurricanes in particular, have basic states that are nearly neutral to slantwise symmetric perturbations (e.g., Emanuel 1986). A necessary condition for the symmetric stability of a cloudy baroclinic vortex, with no secondary circulation, may be written as a local constraint on Υ.

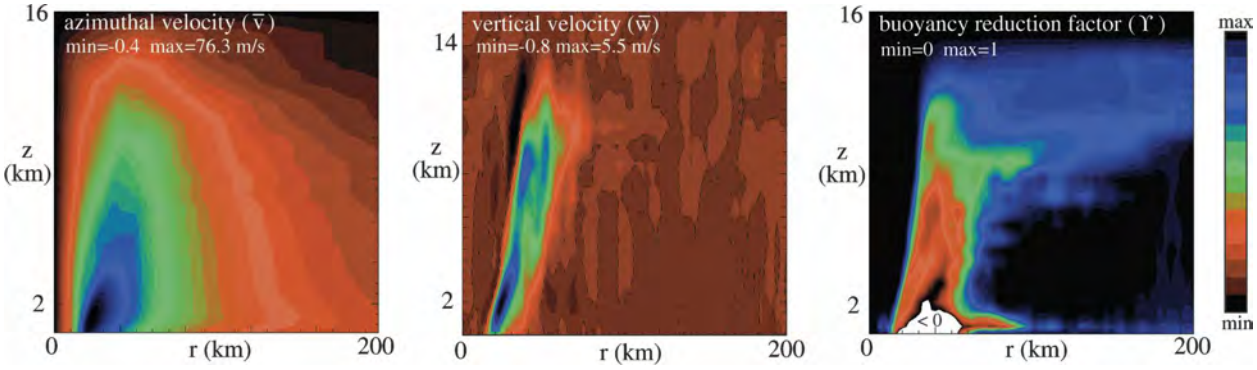

FIG. 2. The (left) azimuthal velocity, (middle) vertical velocity, and (right) buoyancy reduction factor of a mature hurricane, simulated with RAMS. The dashed curves in the vertical velocity plot are zero contours. In all plots, the radius and height axes are scaled linearly. The data set used to produce this figure was kindly provided by Dr. M. Nicholls and Dr. J. Persing.

To begin with, let

$$\frac{\partial}{\partial \varphi} \to 0 \quad \text{and} \quad \frac{1}{r}\frac{\partial (ru')}{\partial r} \to \frac{\partial u'}{\partial r} \tag{35}$$

in Eqs. (29)–(31) and (34). In addition, let

$$\bar{\xi}, \bar{\eta}, \frac{\partial \bar{v}}{\partial p}, \frac{\partial \bar{\theta}_\rho}{\partial r}, \Upsilon \frac{\partial \bar{\theta}_\rho}{\partial p} \to \text{constants}, \tag{36}$$

along with the coefficient of θ_p' on the right-hand side of Eq. (33). The above substitutions are justifiable only if (i) the perturbation is roughly axisymmetric, (ii) the perturbation fields vary much more rapidly than the mean fields with r and p, and (iii) the radial wavelength of the perturbation is much less than r. We will refer to the simplified equations as the local axisymmetric model.

Appendix B shows that perturbations are stable in the local axisymmetric model if and only if

$$\Upsilon \geq \Upsilon_{nt}(r,p) \equiv -\frac{[\bar{\xi}(\partial \bar{v}/\partial p)]^2}{R_d \bar{\eta}\, \bar{\xi}(\partial \bar{\theta}_\rho/\partial p)} p \left(\frac{p_0}{p}\right)^{R_d/c_{pd}}, \tag{37}$$

or equivalently,

$$\left(\frac{\partial \bar{\theta}_\rho}{\partial p}\right)_{\bar{M}} \leq \bar{\chi}, \tag{38}$$

in which the pressure derivative is along a contour of constant angular momentum, $\bar{M} \equiv r\bar{v} + fr^2/2$. For global stability, this condition must hold at every point in the r–p plane (cf. Ooyama 1966).

We have not proven that condition (37) guarantees nongrowth of vortex-scale symmetric perturbations. Nevertheless, if $\Upsilon = \Upsilon_{nt}$, we will casually say that the vortex is neutral to slantwise convection. In section 6, we will see how the growth of an asymmetric perturbation can change as a vortex moistens and becomes neutral to slantwise convection.

It is worth mentioning that even complete cloud coverage can leave sections of a vortex symmetrically stable. Therefore, although setting $\Upsilon = \Upsilon_{nt}$ is of theoretical interest, it is not always physical.

b. Υ for a simulated hurricane

Let us now consider the Υ distribution of a mature hurricane in a "cloud-resolving" numerical simulation. This particular simulation was performed with the Regional Atmospheric Modeling System (RAMS), developed at Colorado State University (see Cotton et al. 2003). It was optionally set to include liquid cloud and rain, but not ice.

Figure 2 shows the instantaneous azimuthal means of the tangential and vertical velocity fields of the simulated hurricane. In addition, it shows the buoyancy reduction factor Υ. To evaluate Υ [the right-hand side of Eq. (32)], we used the instantaneous azimuthal means of θ_ρ and χ.[1] To evaluate χ at each grid point we used Eq. (15), Eq. (16), and the RAMS approximation for $q_{v*}(T, p)$. As expected, Υ is minimal in the main updraft region, where the air is very moist. This region also contains the strongest tangential winds. Low Υ at high $\bar{v}$ is a key result to extract from this figure.

Although tempting, we cannot use the theory of section 5a to properly evaluate the symmetric stability of the RAMS hurricane. Condition (37) strictly applies to a vortex that has no mean secondary circulation. In contrast, the RAMS hurricane is maintained by a strong radial inflow (not shown) that has a peak velocity of about 30 m s^{-1} near the surface. Still, the negative

[1] Because of strong secondary circulation, the azimuthal mean of θ_ρ, averaged over any time interval, does not exactly satisfy the thermal wind equation (28). Therefore, the plotted buoyancy reduction factor differs slightly from the formally defined Υ.

values of Υ at the base of the main updraft might indicate that the vortex is gravitationally unstable in that region.

6. Eyewall instability

The circular eyewall of a mature hurricane can destabilize and evolve into a ring of mesovortices, which itself can destabilize and rapidly spread angular momentum into the eye. This process, the asymmetric instability of a cylindrical vortex sheet, has been studied extensively in laboratory experiments (e.g., Weske and Rankin 1963; Ward 1972; Vladimirov and Tarasov 1980; Montgomery et al. 2002). It has also been studied theoretically/computationally without much consideration of moisture (e.g., Michalke and Timme 1967; Rotunno 1978; Gall 1983; Davidson 1990, chap. 6; Schubert et al. 1999; Kossin and Schubert 2001; Nolan and Montgomery 2002; Terwey and Montgomery 2002). However, hurricane eyewalls are covered with relatively deep clouds (see Fig. 2). In this section, we will examine a case in which such cloud coverage gravely decelerates the linear stage of an asymmetric eyewall instability.

a. Preliminary consideration: The quasigeostrophic shallow-water potential vorticity ring

The shallow-water potential vorticity ring is perhaps the simplest analogue of a mature hurricane. In this analogy, one relates cloud coverage to a reduction of the gravitational restoring force. As a preparatory exercise, we here examine the effect of lowering g (the gravitational acceleration) on the asymmetric breakdown of a shallow-water potential vorticity ring. For analytical simplicity, we confine our discussion to the quasigeostrophic (QG) parameter regime. Although hurricanes have basic states that are ageostrophic, we may expect their vortex-scale shear-flow instabilities to have QG-like properties (e.g., Montgomery and Shapiro 1995). We will return to this matter in section 6c.

In QG theory, fluid motions are assumed to be slow compared to inertial oscillations. Consequently, the dominant component of the velocity field is the divergence-free geostrophic wind,

$$\mathbf{u}_g = -\frac{1}{r}\frac{\partial \psi_g}{\partial \varphi}\hat{\mathbf{r}} + \frac{\partial \psi_g}{\partial r}\hat{\boldsymbol{\varphi}}. \tag{39}$$

Here, we have introduced the geostrophic streamfunction, $\psi_g = gh'/f$, in which h' is the surface-height anomaly of the shallow-water layer.

The dynamics of a QG shallow-water ring is governed by material conservation of PV,

$$\frac{\partial \Pi_{qg}}{\partial t} + \frac{1}{r}\frac{\partial \psi_g}{\partial r}\frac{\partial \Pi_{qg}}{\partial \varphi} - \frac{1}{r}\frac{\partial \psi_g}{\partial \varphi}\frac{\partial \Pi_{qg}}{\partial r} = 0, \tag{40}$$

coupled to an invertibility relation,

$$\left(\frac{1}{r}\frac{\partial}{\partial r}r\frac{\partial}{\partial r} + \frac{1}{r^2}\frac{\partial^2}{\partial \varphi^2} - \frac{1}{l_R^2}\right)\psi_g = \Pi_{qg}. \tag{41}$$

The length scale l_R that appears in the differential operator is the Rossby deformation radius. It is here defined by $l_R \equiv \sqrt{gh_\infty}/f$, in which h_∞ is the ambient surface height.

The unperturbed PV distributions of the rings under consideration have the form

$$\overline{\Pi}_{qg}(r) = Z_0 + Z_1 H(r - r_1) - Z_2 H(r - r_2), \tag{42}$$

in which $r_1 < r_2$, Z_0 and Z_1 are positive, and $Z_2 \equiv Z_0 + Z_1$. As r increases, the PV jumps from Z_0 to $Z_0 + Z_1$ at the radius r_1, and then drops to zero at r_2.

The unperturbed angular rotation frequency is formally given by

$$\overline{\Omega}(r) = \frac{1}{r}\frac{d\overline{\psi}_g}{dr} = \frac{1}{r}\frac{d}{dr}\int_0^\infty d\tilde{r}\tilde{r}G_0(r|\tilde{r})\overline{\Pi}_{qg}(\tilde{r}). \tag{43}$$

The Green function that appears in the radial integral is the $n = 0$ member of the family that is defined by

$$\left(\frac{1}{r}\frac{\partial}{\partial r}r\frac{\partial}{\partial r} - \frac{n^2}{r^2} - \frac{1}{l_R^2}\right)G_n(r|\tilde{r}) \equiv \frac{\delta(r - \tilde{r})}{r}. \tag{44}$$

Requiring regularity at the origin and evanescence as $r \to \infty$, we have

$$G_n(r|\tilde{r}) = -I_n(r_</l_R)K_n(r_>/l_R), \tag{45}$$

in which I_n and K_n are modified Bessel functions, and $r_>(r_<)$ is the greater (lesser) of r and $\tilde{r}$. We note that if Z_0 is zero, $\overline{\Omega}$ is negative in the vortex core. Despite its anticyclonic interior, this shear flow still resembles a mature hurricane in that $\overline{\Omega}$ rapidly increases with radius (to a positive value) between r_1 and r_2, and then decays as r tends to infinity.

In what follows, we will use the notation Ω_1 and Ω_2 to denote the values of $\overline{\Omega}$ at r_1 and r_2, respectively. Using various analytical properties of modified Bessel functions that are, for example, listed in Abramowitz and Stegun (1972), one finds from Eq. (43) that

$$\Omega_1 = Z_1 G_1(r_1|r_1) - Z_2\frac{r_2}{r_1}G_1(r_1|r_2), \tag{46}$$

and

$$\Omega_2 = Z_1\frac{r_1}{r_2}G_1(r_1|r_2) - Z_2 G_1(r_2|r_2). \tag{47}$$

A QG shallow-water ring supports two discrete modes for each azimuthal wavenumber n. Both have the form

$$\Pi'_{qg}(r, \varphi, t) = [\Pi_1 \delta(r - r_1) + \Pi_2 \delta(r - r_2)] e^{i(n\varphi - \nu t)} + \text{c.c.}, \tag{48}$$

in which Π_1 and Π_2 are complex constants, and c.c. denotes the complex conjugate of the preceding term. Evidently, both modes contain a pair of frequency-matched VR waves on opposite edges of the ring. The eigenfrequency is generally complex; that is, $\nu = \nu_R + i\nu_I$, in which ν_R and ν_I are real.

Standard analysis leads to the following modal dispersion relation:

$$\nu_{\pm} = -\frac{b}{2} \pm \frac{1}{2}\sqrt{b^2 - 4c}, \tag{49}$$

in which

$$b \equiv n[Z_1 G_n(r_1|r_1) - Z_2 G_n(r_2|r_2) - (\Omega_1 + \Omega_2)], \tag{50}$$

and

$$c \equiv n^2\{\Omega_1\Omega_2 + \Omega_1 Z_2 G_n(r_2|r_2) - \Omega_2 Z_1 G_n(r_1|r_1) + Z_1 Z_2[G_n(r_1|r_2)^2 - G_n(r_1|r_1)G_n(r_2|r_2)]\}. \tag{51}$$

If $n = 1$, it can be shown that $c = 0$ and the discrete modes are neutral. For $n \geq 2$, there will exist a growing mode and a conjugate damped mode if the discriminant $b^2 - 4c$ is negative.

With the aid of symbolic computation,[2] we have found that

$$c \sim -\frac{l_R^6 n^2 (n^2 - 1)^2 Z_1 Z_2}{16 r_1^3 r_2^3} < 0 \tag{52}$$

as $l_R \to 0$. Therefore, any growing mode will neutralize as the deformation radius drops below a finite threshold. Such stabilization occurs in part because the VR waves on opposite edges of the ring become shielded from each other, and can no longer interact effectively. Of course, for more subtle reasons the growth rate may vary nonmonotonically with decreasing l_R before shooting to zero.

Figure 3 illustrates the typical properties of an unstable mode of a shallow-water PV ring. The angular phase velocity of the mode is greater than Ω_1 but less than Ω_2. Therefore, the inner VR wave is prograde, whereas the outer VR wave is retrograde. As predicted, the mode neutralizes as the gravitational restoring force (parameterized by l_R) drops below a finite threshold.[3]

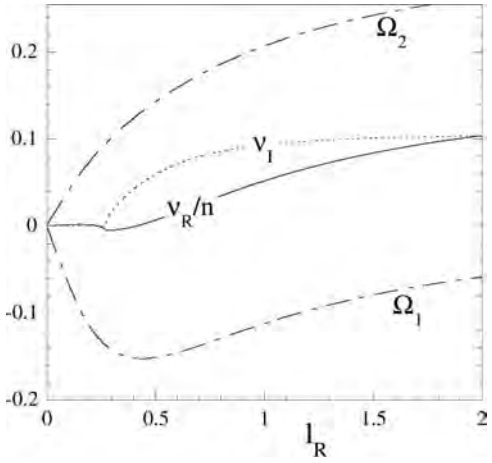

FIG. 3. The l_R dependence of the complex frequency of the $n = 3$ growing mode of a QG shallow-water ring, with $r_1 = 3/4$, $r_2 = 5/4$, $Z_2 = Z_1 = 1$, and thus $Z_0 = 0$. Because the phase velocity ν_R/n is between Ω_1 and Ω_2, the inner VR wave is prograde, whereas the outer VR wave is retrograde. Note also that the growth rate ν_I is zero for all l_R below a finite threshold.

b. A category 3 hurricane

We now reexamine the eyewall instability of the category 3 "hurricane" in Nolan and Montgomery (2002, hereafter NM02). The reader may consult NM02 for an analytical description of the basic-state cyclonic vorticity $\bar{\zeta}(r, z)$. The vorticity is easily integrated for azimuthal velocity $\bar{v}(r, z)$. The equilibrium profiles of pressure and density, $\bar{p}(r, z)$ and $\bar{\rho}(r, z)$, are found by an iterative algorithm that solves hydrostatic and gradient wind balance simultaneously. For this study, a Jordan mean sounding gives the thermal boundary condition at $r = 200$ km (Jordan 1958). In addition, the Coriolis parameter is set to $f = 5 \times 10^{-5}\ \text{s}^{-1}$. Figure 4 portrays the basic state of the vortex on the r–p plane. Note that the eyewall (where $\bar{v}$ peaks) has a ringlike PV distribution of finite depth.[4]

[2] To begin with, all modified Bessel functions in the definition of c were replaced with the first seven terms of their large-argument (small l_R) asymptotic expansions (Abramowitz and Stegun 1972). The resulting approximation for c was then reduced to a manageable size with the "Simplify" routine of Mathematica 5.0. Equation (52) is the leading-order term of the approximation.

[3] By very similar analysis, it is readily shown that, in the context of QG theory, the internal VR modes of a density-stratified barotropic PV ring ultimately stabilize as the buoyancy frequency tends toward zero.

[4] "Cloud-resolving" numerical simulations suggest that the midlevel PV of a mature hurricane is more broadly distributed in radius (e.g., Chen and Yau 2001). So, in the middle troposphere, the sharply peaked PV profile of the NM02 hurricane might be atypical. Observations of Isabel 2003 further show that the PV distribution of a real hurricane can have multiple maxima (Bell and Montgomery 2006, manuscript submitted to *Mon. Wea. Rev.*). We leave this more complex situation for future consideration.

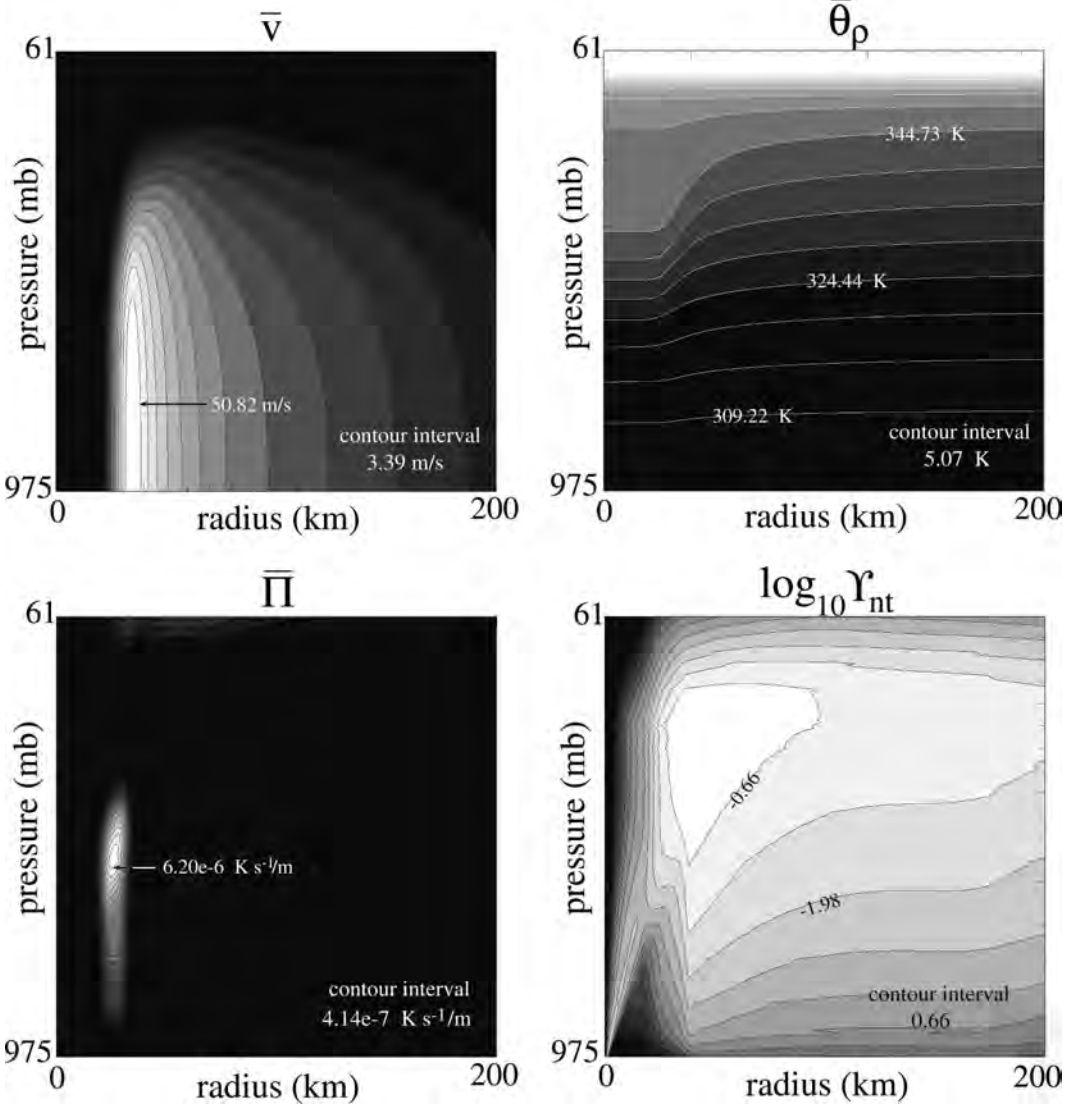

FIG. 4. Basic state of the Nolan–Montgomery category 3 hurricane. Contours ranging from 380.23 to 466.46 K were removed from the stratosphere of the $\overline{\theta}_\rho$ plot due to excessive bunching. In all plots, the radius and pressure axes are scaled linearly.

According to NM02, if the vortex is dry, its eyewall is unstable. Moreover, the azimuthal wavenumber of the fastest growing eigenmode is $n = 3$. In order to understand how moisture influences the fastest growing mode, we here consider a set of numerical experiments with variable Υ. Specifically, we let

$$\Upsilon(r, p) = 1 - \varepsilon[1 - \Upsilon_{nt}(r, p)]. \tag{53}$$

As the single parameter ε increases from zero to one, the vortex goes from a dry state to a moist state that is neutral to slantwise convection. The lower right panel of Fig. 4 shows Υ_{nt} for the vortex under consideration.

In each experiment, the vortex is initialized with an arbitrary $n = 3$ perturbation. Appendix C describes the numerical model that is used to evolve the disturbance forward in time. In all cases, a growing eigenmode prevails after a brief adjustment period. To be clear, the eigenmode is a disturbance of the form

$$\phi' = \Phi(r, p)e^{i(n\varphi - \nu t)} + \text{c.c.}, \tag{54}$$

and likewise for all other perturbation fields. As before, $\nu \equiv \nu_R + i\nu_I$, in which ν_R and ν_I are real. Figure 5 illustrates the exponential growth of the mode for in-

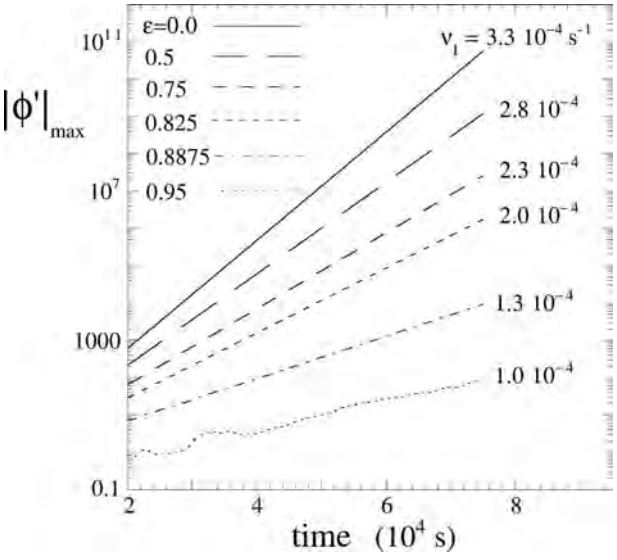

FIG. 5. Domain maximum of the $n = 3$ geopotential perturbation of the NM02 hurricane, with variable moisture. After a brief transition period, the perturbation grows like $e^{\nu_I t}$. The values of ν_I are given to the right of each curve. As additional moisture (increasing ε) brings the vortex toward slantwise convective neutrality, the instability slows down. In this plot, $|\phi'|_{max}$ is normalized to its initial value.

creasing levels of moisture. Evidently, cloud coverage tends to neutralize the mode.[5]

We note that the growth rate of the dry mode (3.3×10^{-4} s^{-1}) exceeds the value of 2.07×10^{-4} s^{-1} that appears in NM02. During the review process, D. Nolan (2006, personal communication) was able to repeat the computation of NM02 at a finer spatial resolution, which is now practical. With more than double the number of radial grid points, the growth rate of the dry mode increased to 2.7×10^{-4} s^{-1}. The remaining discrepancy between this value and our result is likely caused by (i) our different surface boundary condition ($\omega' = 0$ on a constant p surface as opposed to no stress on a constant z surface), (ii) our use of the hydrostatic approximation, and (iii) the absence of explicit eddy diffusion in our model.

c. Comparison

In many ways, the eyewall instability of the NM02 hurricane resembles the instability of a QG shallow-water ring. To begin with, whether dry or moist, the unstable eyewall mode of the NM02 hurricane appears to comprise counter propagating VR waves.[6] To see this, let us examine its structure. The time-asymptotic PV perturbation approximately has the form

$$\Pi' = \hat{\Pi}(r, p)e^{i(n\varphi - \nu t)} + \text{c.c.} \tag{55}$$

The two plots in Fig. 6 show $|\hat{\Pi}|$ for $\varepsilon = 0$ and for $\varepsilon = 0.8875$. For $\varepsilon = 0$, the dry case, the radial variation of $|\hat{\Pi}|$ has two distinct peaks. These peaks occur at the maximum positive and negative values of $\partial\overline{\Pi}/\partial r$. For $\varepsilon = 0.8875$, $|\hat{\Pi}|$ has a similar structure, but the inner wave is fractured.

In both plots, the dashed arc is where the Doppler-shifted mode frequency,

$$\sigma_R(r, p) \equiv \nu_R - n\overline{\Omega}, \tag{56}$$

is zero. Above the arc $\sigma_R > 0$, and below the arc $\sigma_R < 0$. Whether dry or moist, the inner wave is above the arc, and is therefore prograde relative to the mean flow. In contrast, the outer wave is underneath the arc, and is therefore retrograde. These properties are consistent with the azimuthal propagation rule for VR waves in a cyclone: the propagation is prograde/retrograde if $\partial\overline{\Pi}/\partial r$ is positive/negative (Montgomery and Kallenbach 1997).

True VR waves should also be slow, in some sense, relative to IG oscillations. One quantitative condition for slowness is given below:

$$\mathcal{D}^2 \equiv \frac{\sigma_R^2}{\dfrac{(\bar{\xi}\partial\bar{v}/\partial p)^2}{\Upsilon\partial\bar{\theta}_\rho/\partial p}\dfrac{p}{R_d}\left(\dfrac{p_0}{p}\right)^{R_d/c_{pd}} + \bar{\eta}\bar{\xi}} \ll 1. \tag{57}$$

The above condition states that the Doppler-shifted mode frequency should be much less than the minimum frequency of slantwise IG oscillations (the square root of the denominator; see appendix B). The contours in Fig. 6 show the r–p variation of $\mathcal{D}^2$ for the dry and moist modes. In the eyewall, both modes appear to marginally satisfy condition (57).[7]

We note that if $\mathcal{D}^2 \ll 1$, terms of order $\mathcal{D}^2$ and higher are subdominant in the perturbation equations. Neglecting these terms leads to the zero-order asymmetric balance model (Shapiro and Montgomery 1993; Montgomery and Shapiro 1995; Montgomery and Franklin 1998; Ren 1999; McWilliams et al. 2003). Like QG theory, the asymmetric balance model filters out inertia–gravity waves. Unlike QG theory, the basic state can have a Rossby number of order unity or greater.

[5] Dunkerton (1990) examined a similar divergent barotropic instability of a zonal shear flow. By comparison, he showed that the growth rate of the instability can first increase and then decrease as the static stability of the atmosphere tends toward zero by, say, increasing cloudiness.

[6] Nolan and Montgomery (2002) discuss the Rossby wave nature of the instability for the dry case. The objective here is to extend the discussion to cases in which clouds are present.

[7] We should point out that as $\Upsilon \to \Upsilon_{nt}$, $\mathcal{D}^2$ becomes infinite everywhere but on the contour $\sigma_R = 0$. Therefore, the area in which condition (57) holds must vanish as $\varepsilon \to 1$.

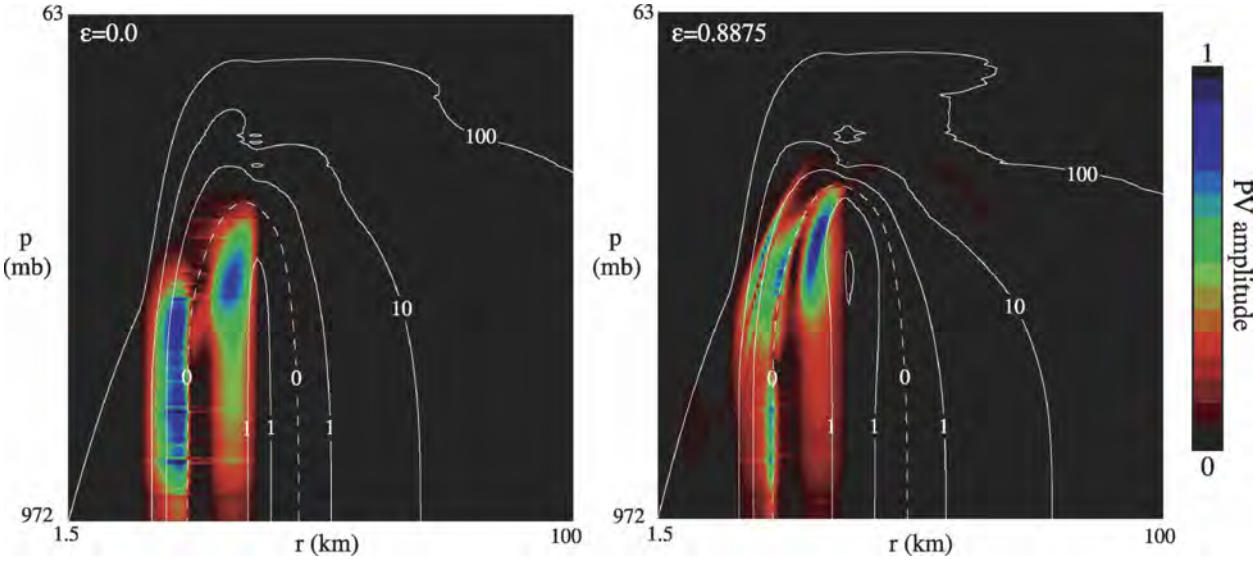

FIG. 6. The PV amplitude $|\hat{\Pi}|$ (normalized to its maximum) and slowness parameter $\mathcal{D}^2$ (contours) for the most unstable $n = 3$ eyewall modes of a dry and a moist NM02 hurricane. In both plots, the radius and pressure axes are scaled linearly.

In summary, the pertinent instabilities of a QG shallow-water ring and of the NM02 hurricane both consist of slow, counter propagating VR waves. By analogy to the QG shallow-water ring, it is no surprise that reduction of the gravitational/buoyancy restoring force by adding moisture suppresses the NM02 hurricane instability.

Of course, the analogy has limits. To begin with, the NM02 hurricane mode is not globally slow, as it is in QG theory. Figure 6 indicates severe violation of condition (57) in the periphery of the storm, in the eye of the storm, and in the upper troposphere. Previous studies have shown that such external violation can, in some cases, notably affect the growth rate of a vortex mode (Schecter and Montgomery 2003). Furthermore, moisture significantly alters the r–p structure of the mode. Figure 6 alone illustrates a vertical elevation and scale reduction of PV peaks. Figure 7 illustrates the changes of other perturbation fields. Note in particular that moisture causes mesoscale spatial oscillations to emerge in the eye. The emergence is most striking for ω'.[8]

7. The eigenmode problem for a cloudy vortex

In section 8, we will examine the discrete eigenmodes of a cloudy vortex that resembles an incipient tropical cyclone. Before doing so, it is helpful to discuss the eigenmode problem more generally.

a. Eigenmode problem for a generic vortex

Substituting a traveling wave ansatz [Eq. (54) and relatives] into the linearized equations of motion [Eqs. (29)–(34)], and eliminating all perturbation fields but the geopotential, we obtain

$$\frac{1}{r}\frac{\partial}{\partial r}\left(\frac{r}{\Gamma}\Upsilon\frac{\partial\bar{\theta}_\rho}{\partial p}\frac{\partial\Phi}{\partial r}\right)+\frac{\partial}{\partial p}\left[\frac{\bar{\psi}p}{R_d\Gamma}\left(\frac{p_0}{p}\right)^{R_d/c_{pd}}\frac{\partial\Phi}{\partial p}\right]-\frac{2}{\Gamma}\frac{\partial\bar{\theta}_\rho}{\partial r}\frac{\partial^2\Phi}{\partial p\partial r}-\frac{\partial}{\partial p}\left(\frac{1}{\Gamma}\frac{\partial\bar{\theta}_\rho}{\partial r}\right)\frac{\partial\Phi}{\partial r}-\frac{1}{r}\frac{\partial}{\partial r}\left(\frac{r}{\Gamma}\frac{\partial\bar{\theta}_\rho}{\partial r}\right)\frac{\partial\Phi}{\partial p}$$
$$-\frac{n^2}{r^2\Gamma}\Upsilon\frac{\partial\bar{\theta}_\rho}{\partial p}\Phi+\frac{1}{r\sigma}\left[\frac{\partial}{\partial p}\left(\frac{n\bar{\xi}}{\Gamma}\frac{\partial\bar{\theta}_\rho}{\partial r}\right)-\frac{\partial}{\partial r}\left(\frac{n\bar{\xi}}{\Gamma}\Upsilon\frac{\partial\bar{\theta}_\rho}{\partial p}\right)\right]\Phi=0, \tag{58}$$

in which

$$\sigma\equiv\nu-n\bar{\Omega}, \tag{59}$$

is the complex Doppler-shifted mode frequency,

$$\bar{\psi}\equiv\sigma^2-\bar{\eta}\,\bar{\xi}, \tag{60}$$

and

$$\Gamma\equiv\bar{\psi}\Upsilon\frac{\partial\bar{\theta}_\rho}{\partial p}-\left(\bar{\xi}\frac{\partial\bar{v}}{\partial p}\right)^2\frac{p}{R_d}\left(\frac{p_0}{p}\right)^{R_d/c_{pd}}. \tag{61}$$

[8] A more realistic representation of a hurricane would have a relatively dry eye compared to the eyewall, in which case the striking fluctuations of ω' at small radii would likely disappear.

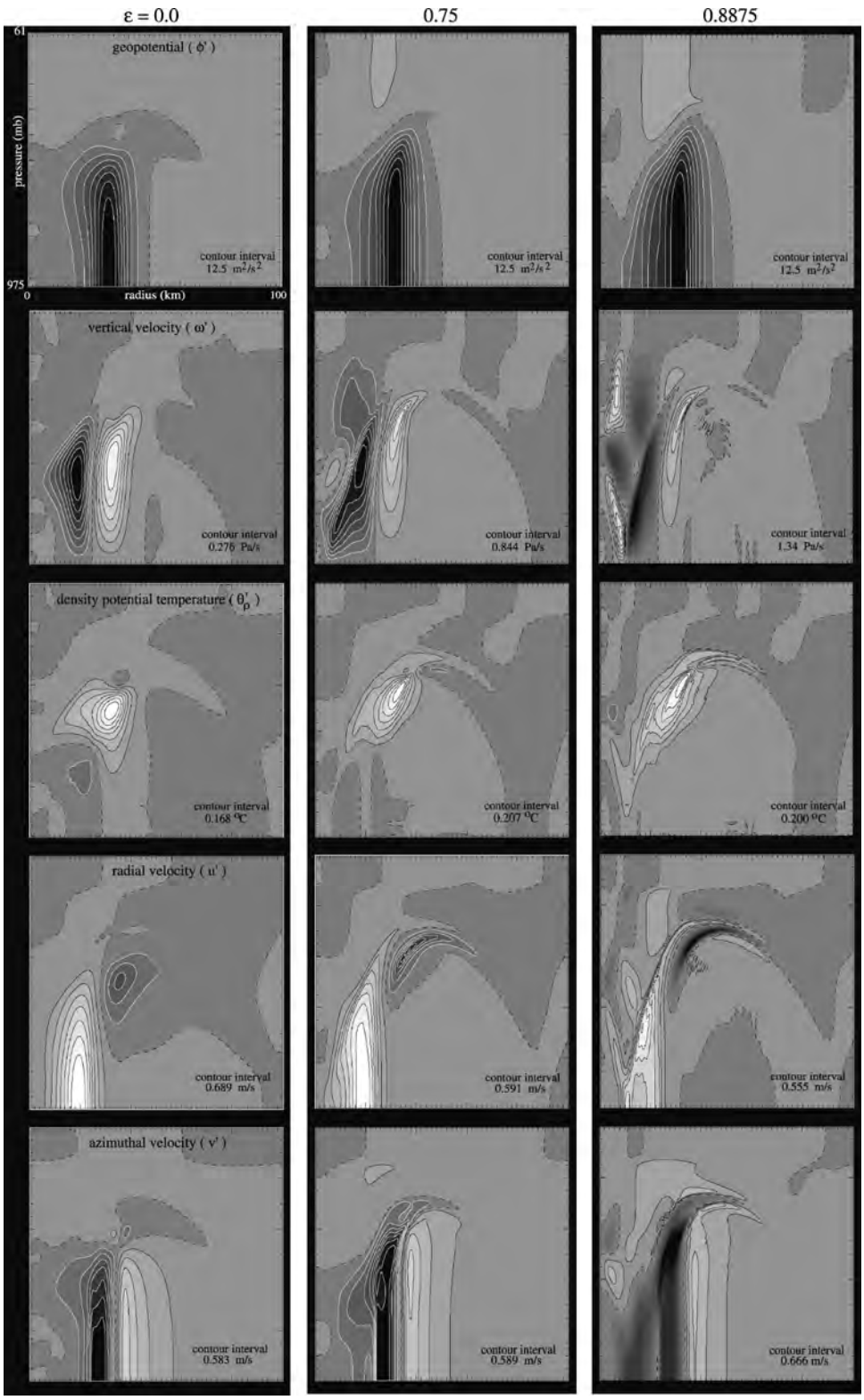

FIG. 7. Vertical slices of the unstable $n = 3$ eyewall mode of the NM02 hurricane, for increasing levels of moisture from left to right. The radius and pressure axes are scaled linearly, and have the same limits for every plot (see top left). The azimuth (φ) for each column is where θ'_ρ has its peak value. The wave amplitudes are arbitrarily normalized so that the maximum of $|\phi'|$, at the azimuth shown, is 100 $m^2\ s^{-2}$. Bright (dark) shades represent positive (negative) values of the plotted fields. The dashed curves are the zero contours. Because of excessive bunching, negative contours were removed from the $\varepsilon = 0.8875$ velocity plots.

The values of ν that permit nontrivial solutions of Eq. (58), that is, the eigenfrequencies, are constrained by the radial and vertical (pressure) boundary conditions. We will specify these conditions when the need arises.

b. *Eigenmode problem for a barotropic vortex with separable* Υ

Equation (58) is complicated, and useful only if simplified. For example, suppose that the basic state of the vortex is barotropic; that is,

$$\frac{\partial \bar{v}}{\partial p}, \frac{\partial \bar{\theta}_\rho}{\partial r} = 0. \tag{62}$$

Then, the eigenmode equation reduces to the following:

$$\frac{1}{r}\frac{\partial}{\partial r}\left(\frac{r}{\bar{\psi}}\frac{\partial \Phi}{\partial r}\right) - \frac{1}{r\sigma}\frac{d}{dr}\left(\frac{n\bar{\xi}}{\bar{\psi}}\right)\Phi - \frac{n^2}{r^2\bar{\psi}}\Phi + L(\Phi) = 0, \tag{63}$$

in which

$$L(\Phi) \equiv \frac{\partial}{\partial p}\left[\frac{p}{R_d \Upsilon d\bar{\theta}_p/dp}\left(\frac{p_0}{p}\right)^{R_d/c_{pd}}\frac{\partial \Phi}{\partial p}\right]. \tag{64}$$

Further suppose that the buoyancy reduction factor is separable. Then, we may write

$$\Upsilon \frac{d\bar{\theta}_\rho}{dp} = \mathcal{R}(r)\mathcal{P}(p). \tag{65}$$

Equation (65) permits us to seek eigenfunctions of the form

$$\Phi = \Phi_\lambda(r)\Psi_\lambda(p). \tag{66}$$

Upon substituting Eq. (66) into Eq. (63), we find that a nontrivial solution for Φ_λ can exist only if

$$\frac{d}{dp}\left[\frac{p}{R_d\mathcal{P}(p)}\left(\frac{p_0}{p}\right)^{R_d/c_{pd}}\frac{d\Psi_\lambda}{dp}\right] = \lambda\Psi_\lambda, \tag{67}$$

in which λ is a constant. The vertical boundary conditions determine the permissible values of λ. Higher values of λ correspond to eigenfunctions with smaller vertical wavelengths. If, for example, $\omega' = 0$ at $p = p_{\min}$ and at $p = p_{\max}$, then the boundary conditions are $d\Psi_\lambda/dp = 0$ at $p = p_{\min}$ and at $p = p_{\max}$.

Inserting Eqs. (65)–(67) into Eq. (63), and dividing through by Ψ_λ yields

$$\frac{1}{r}\frac{\partial}{\partial r}\left(\frac{r}{\bar{\psi}}\frac{\partial \Phi_\lambda}{\partial r}\right) - \frac{1}{r\sigma}\frac{d}{dr}\left(\frac{n\bar{\xi}}{\bar{\psi}}\right)\Phi_\lambda - \frac{n^2}{r^2\bar{\psi}}\Phi_\lambda + \frac{1}{l_R^2 f^2}\Phi_\lambda = 0. \tag{68}$$

The symbol l_R here denotes the internal Rossby deformation radius, defined by

$$l_R = \sqrt{\frac{\mathcal{R}}{f^2\lambda}}. \tag{69}$$

Clearly, l_R decreases as the vertical wavenumber or the Coriolis parameter increases; l_R also varies radially.

Suppose that $\mathcal{P} = cd\bar{\theta}_\rho/dp$, in which c is a constant. Then,

$$l_R = \sqrt{\Upsilon(r)}\, l_R^{\text{dry}}, \tag{70}$$

in which l_R^{dry} is the internal Rossby deformation radius in the absence of moisture. Since $\Upsilon \le 1$, it is clear that moisture reduces l_R.

To complete the eigenmode problem, we must specify two radial boundary conditions. At the origin, we require that Φ_λ is zero ($n \ge 1$) or finite ($n = 0$). As $r \to \infty$, we impose either a radiation or evanescence condition, depending on whether the mode is fast or slow relative to an ambient inertial oscillation. In appendix D, we give both the inner and outer asymptotic forms of Φ_λ. From these, we can infer relations between Φ_λ and $d\Phi_\lambda/dr$ near the origin and at distant radii. We use these relations for mixed boundary conditions in our numerical eigenmode solver, which is based on the shooting method. The computational boundaries are typically at $0.01r_o$ and $15r_o$, in which r_o is the radius of the vortex core.

Interested readers may consult appendix E for a set of polarization equations that give the wavefunctions for u', v', and θ'_ρ in terms of $\Phi_\lambda(r)$ and $\Psi_\lambda(p)$.

8. Suppression of spiral inertia–gravity wave radiation and improvement of vortex resilience by cloud coverage

During their early stages of development, and perhaps after eyewall breakdown, tropical cyclones are presently thought to have PV distributions that, roughly speaking, decrease monotonically away from the storm center. In this section, we examine how moisture affects the propagation and exponential growth of discrete VR waves in an ageostrophic monotonic cyclone. The most familiar of these waves include rotating tilts and elliptical deformations (e.g., Kelvin 1880; Schecter and Montgomery 2004). They are distinguished from continuum VR waves (e.g., Montgomery and Kallenbach 1997; Bassom and Gilbert 1998) in that their PV fields do not characteristically suffer spiral windup. Typically, spiral windup of PV leads to algebraic decay of the asymmetric geopotential perturbation, as opposed to exponential decay or growth.

Discrete VR waves have some role in regulating tropical cyclone intensity. This role is not completely understood, but some basic theory has been developed.

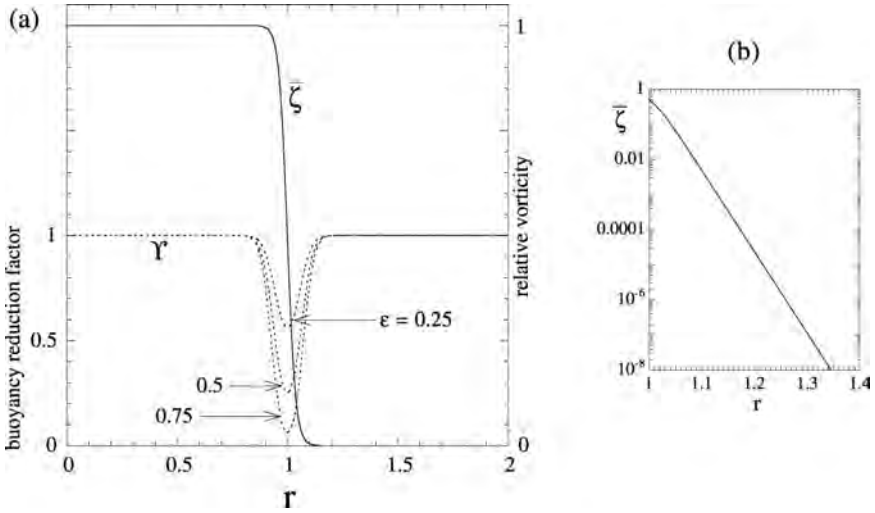

FIG. 8. A tanh barotropic cyclone with variable cloudiness. (a) Relative vorticity $\overline{\zeta} = \overline{\eta} - f$, and buoyancy reduction factor Υ for increasing levels of moisture (increasing ε) near the radius of maximum wind. (b) The outer relative vorticity has a small but finite negative gradient. In both (a) and (b), $\overline{\zeta}$ is normalized to its central value, and r is normalized to the core radius r_o.

In linear theory, discrete VR waves are compelled to decay by resonant transfer of wave activity into a critical layer (Briggs et al. 1970; Pillai and Gould 1994; Schecter et al. 2000, 2002; Balmforth et al. 2001; Schecter and Montgomery 2004, 2006; Mallen et al. 2005). During decay, the wave–mean flow interaction usually increases the maximum tangential wind speed in the vortex core (e.g., Montgomery and Enagonio 1998; Reasor and Montgomery 2001). On the other hand, if $\nu_R > f$, discrete VR waves are compelled to grow by exciting outward propagating spiral IG waves in the environment (Ford 1994a,b; Plougonven and Zeitlin 2002; Schecter and Montgomery 2004, 2006). This spontaneous radiation transports energy and angular momentum away from the vortex. The following demonstrates that core moisture increases the absorption rate of wave activity in the critical layer (indirectly) and thereby inhibits spontaneous IG wave radiation. In this sense, moisture can fortify the cyclone's intensity.

The following demonstration also implies that cloud coverage improves the resilience of a monotonic cyclone that is exposed to ambient vertical shear. Suppose that the discrete VR wave under consideration is a tilt mode ($n = 1$). As mentioned previously, adding clouds to the cyclone either causes or accelerates decay of that mode. Therefore, a cloudy monotonic cyclone realigns more rapidly than its dry counterpart after it is tilted by transient vertical shear. As we will see, cloud coverage also boosts the azimuthal phase velocity of the mode. Intuition and basic modeling suggest that sustained vertical shear becomes relatively harmless if the phase velocity of the mode becomes greater than the shear rate (e.g., Jones 1995; Reasor et al. 2004).

a. A barotropic cyclone

We focus the present study on the discrete VR waves of a barotropic cyclone, with

$$\overline{\zeta}(r) = 2f\left[1 - \tanh\left(\frac{r - r_o}{d}\right)\right]. \tag{71}$$

As r increases from the origin, $\overline{\zeta}$ stays roughly constant, until dropping rapidly toward zero near r_o (see Fig. 8). The width of the transition layer is of order $d = 0.0375r_o$. The Rossby number of the cyclone, $\mathrm{Ro} \equiv \overline{\zeta}(0)/f = 4$, is characteristic of an incipient storm. Most importantly, it exceeds unity. The angular rotation frequency $\overline{\Omega}$ (not shown) is roughly constant for $r < r_o$, and decays nearly as r^{-2} for $r > r_o$.

We further assume that the buoyancy reduction factor does not vary with p. Specifically, we let

$$\Upsilon(r) = [1 - \varepsilon e^{-(r-r_o)^2/(2d)^2}]^2, \tag{72}$$

which has the minimum value $(1 - \varepsilon)^2$ at r_o, and is unity for $|r - r_o| \gg 2d$ (see Fig. 8). The ε parameter can have any value between zero and one. Note that our choice of Υ is minimal in the region of maximum azimuthal wind speed. This property was motivated by the simulated hurricane data in Fig. 2.

b. The growth rate of a discrete vortex Rossby wave

Figure 9 shows a horizontal slice of the geopotential perturbation ϕ' of a discrete VR wave in a cloudy tanh cyclone [Eqs. (71)–(72)]. The oscillation frequency ν_R of the wave exceeds the Coriolis parameter f. Consequently, the VR wave resonantly excites an outward-propagating spiral IG wave in the environment. The coupled VR and IG waves constitute a single eigenmode.

It has been shown that, near marginal stability, the growth rate of a discrete VR wave in a *dry* barotropic vortex is given by the formula (cf. Schecter and Montgomery 2004)

$$\nu_I = \nu_{\rm rad} - \nu_{cl}, \tag{73}$$

in which

$$\nu_{\rm rad} \equiv \frac{r_v^2}{M}\,\Re[U_\lambda V_\lambda^*], \tag{74}$$

and

$$\nu_{cl} = -\frac{\pi}{M}\left[\frac{r^2|U_\lambda|^2 d\overline{\eta}/dr}{|nd\overline{\Omega}/dr|}\right]_{r=r_*}. \tag{75}$$

Here, $U_\lambda(r)$ and $V_\lambda(r)$ are the radial wavefunctions of the radial and azimuthal velocities [see appendix E for their connection to $\Phi_\lambda(r)$]. The superscript * is the complex conjugate operator, and $\Re[\ldots]$ is the real part of the quantity in square brackets. The critical radius r_* is defined by

$$\overline{\Omega}(r_*) \equiv \nu_R/n. \tag{76}$$

It is where the angular rotation frequency of the vortex equals the angular phase velocity of the wave. The radius r_v defines the outer vortex boundary. Its exact value is somewhat arbitrary, but must exceed r_*. The denominator M is defined by

$$M \equiv -\fint_0^{r_v} dr\left[r^2\frac{d\overline{\eta}}{dr}\frac{|U_\lambda|^2}{|\sigma|^2} + \frac{r^2}{f^2 l_R^2}(\Phi_\lambda V_\lambda^* + \text{c.c.})\right], \tag{77}$$

in which $\fint$ denotes a radial integral that excludes an "infinitesimal" band at r_*. Provided that our choice of r_v is not orders of magnitude greater than r_*, M is generally positive (Schecter and Montgomery 2004, 2006). Vertical boundaries do not appear explicitly in the equations above. However, the hidden vertical boundary conditions are $\omega' = 0$ (and hence $\theta_\rho' = 0$) at $p = p_{\rm max}$ and at $p = p_{\rm min}$.

Equation (73) indicates that the growth rate of a discrete VR wave has two parts. The first term, $\nu_{\rm rad}$, is proportional to the outward angular momentum flux of the spiral IG wave that the discrete VR wave emits into the environment. This flux is generally positive; therefore, the IG wave emission destabilizes the discrete VR wave. The second term, $-\nu_{cl}$, accounts for the resonant feedback of PV stirring in the critical layer. It is negative, since $d\overline{\eta}/dr = d\overline{\zeta}/dr < 0$, and therefore acts to stabilize the discrete VR wave.

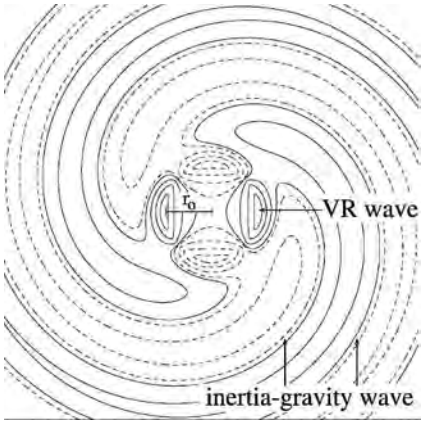

FIG. 9. Horizontal slice of the geopotential perturbation ϕ' of the $n = 2$ discrete VR wave of a tanh barotropic cyclone (Fig. 8), and the IG wave radiation that it generates. The moisture parameter for this case is $\varepsilon = 0.725$, the Rossby number is Ro = 4, and the dry Rossby deformation radius is $l_R^{\rm dry} = r_o$. Solid/dashed contours correspond to positive/negative values of ϕ'. The contour levels are ± 0.05, ± 0.3, ± 0.75, and ± 1.5, in units that are normalized to one-half the amplitude of ϕ' at $r = r_o$.

The preceding growth rate formula also applies to the discrete VR waves of a cloudy barotropic vortex in which Υ is separable [see Eq. (65)]. Moisture implicitly changes the right-hand side of Eq. (73) by altering the wavefunctions, moving r_*, and giving l_R radial variation [see Eq. (70)]. Readers who would like to verify Eq. (73) in the moist context may follow the dry derivation in Schecter and Montgomery (2004). In doing so, one must replace the dry Boussinesq wave activity equation with its moist non-Boussinesq counterpart. Appendix F provides the pertinent equation.

c. Computational results

Figures 10 and 11 illustrate the effects of moisture on the discrete VR waves of the tanh cyclone that is under consideration [Eqs. (71) and (72)]. These waves correspond to (nonsingular) numerical solutions of the eigenmode problem of section 7b. Figure 10 shows how the critical radii vary with the moisture parameter ε. The four plots cover azimuthal wavenumbers 1–4. The different curves in each plot correspond to different values of the dry Rossby deformation radius, $l_R^{\rm dry}$. In

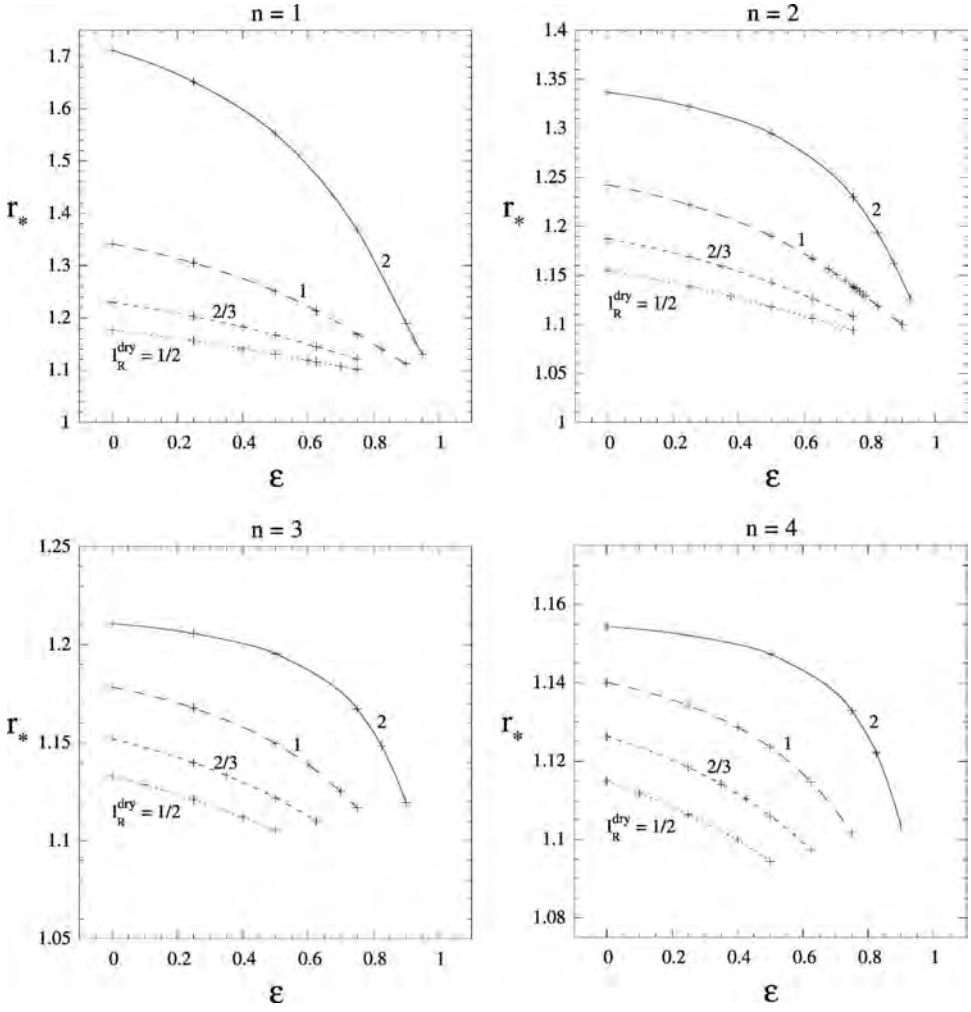

FIG. 10. Critical radius r_* vs the moisture parameter ε for a spectrum of discrete VR waves of a tanh barotropic cyclone, with Ro = 4. In general, r_* decreases toward the core radius r_o of the cyclone as the level of moisture increases. All lengths are normalized to r_o.

general, adding clouds increases the azimuthal phase velocity of a wave and thereby decreases r_* toward r_0.[9]

Figure 11 shows how the growth rates vary with ε. In general, adding clouds tends to decrease ν_I and stabilize a wave. Stabilization occurs because cloud coverage brings the critical radius to a region of relatively large negative PV gradient ($d\overline{\eta}/dr$). This enables critical layer damping to prevail over radiative pumping (see below).

Figure 12 verifies the analytical growth rate formula of section 8b for a particular VR wave that is near marginal stability. Again, the growth rate is plotted as a function of cloudiness in the cyclone. The $\times$ symbols correspond to Eq. (73). To evaluate the right-hand side of this equation, we used the wavefunctions (U_λ, V_λ, Φ_λ) and critical radius (r_*) of the computed eigenmode. To evaluate M, we removed the interval $|r - r_*| < 20|\nu_I/nd\overline{\Omega}/dr_*|$ from the integral; that is, we removed an estimate of the linear critical layer (cf. Schecter et al. 2000; Schecter and Montgomery 2004). Evidently, Eq. (73) accurately reproduces the values of ν_I (+ symbols) that are obtained directly from the eigenmode solutions.

Figure 12 also shows how the radiative pumping rate (ν_{rad}) and critical layer damping rate ($-\nu_{cl}$) vary with the moisture parameter ε. To obtain these rates, ν_{rad} and ν_{cl} were evaluated with $r_v = 3r_o$. As ε increases from zero to one, the radiative pumping rate remains roughly constant. However, the negative PV gradient at r_* explosively

[9] Note that increasing the phase velocity of a discrete VR wave corresponds to slowing its retrograde propagation relative to the mean flow in the vortex core.

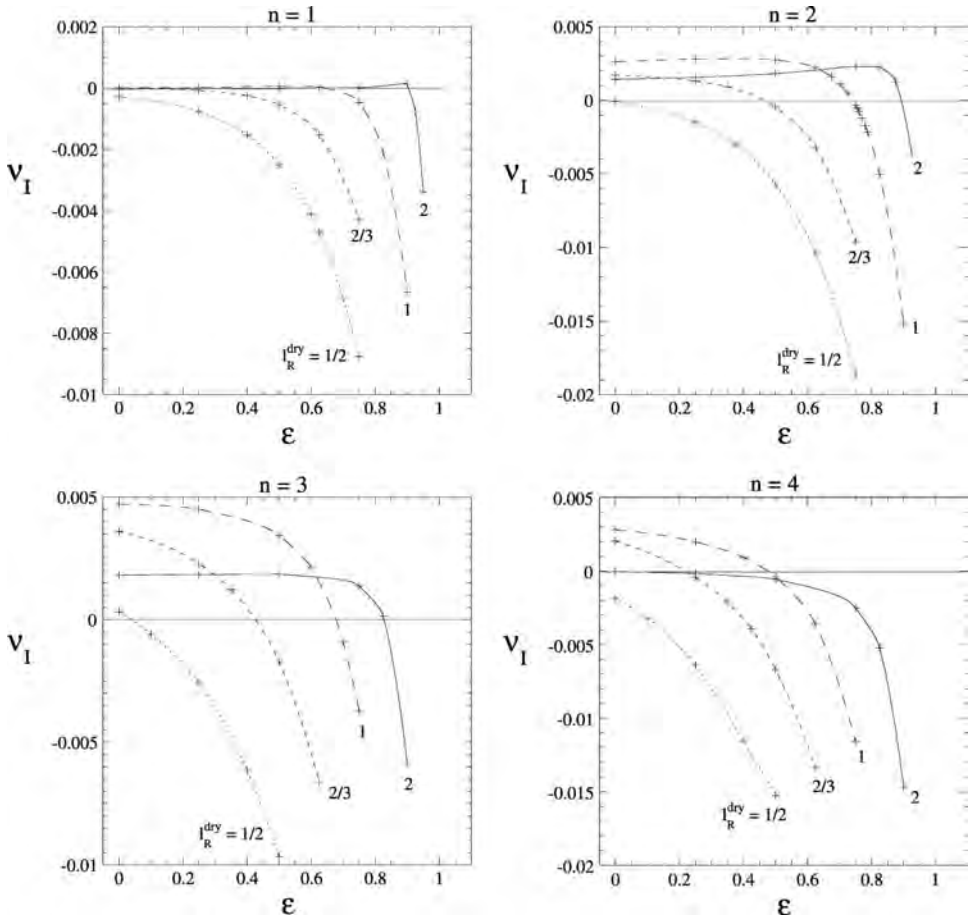

FIG. 11. Growth rate ν_I [normalized to $\bar{\zeta}(0)$] vs the moisture parameter ε for a spectrum of discrete VR waves of a tanh barotropic cyclone, with Ro = 4. In all cases, ν_I eventually becomes negative as the level of moisture increases. All deformation radii are normalized to the core radius r_o.

grows, and the critical layer damping rate increases by orders of magnitude. Consequently, ν_I becomes negative.

We note that as the growth rate becomes negative, the discrete VR wave transforms from an eigenmode into a quasimode. Quasimodes are not exact solutions to the eigenmode problem. For instance, the PV disturbance of a quasimode grows with time in the thin critical layer centered at r_*; in contrast, the PV disturbance of a damped eigenmode would decay everywhere. The numerical method for finding quasimodes is similar to the numerical method for finding eigenmodes, and has been described elsewhere (e.g., Spencer and Rasband 1997; Schecter and Montgomery 2004, 2006).

We must also emphasize that the above discussion is based on linear theory. Nonlinear processes can revive a linearly damped VR wave. For instance, dry studies have shown that radiative pumping ultimately overtakes critical layer damping if the initial VR wave amplitude exceeds a finite threshold (Schecter and Montgomery 2006).

9. Concluding remarks

In this paper, we presented a basic model for small-amplitude wave dynamics in a cloudy vortex. The wave equations were derived with the following set of approximations:

(i) an air parcel conserves its total water content (liquid plus vapor);
(ii) the mixing ratios of water vapor and liquid cloud in an air parcel instantaneously adjust to min[q_t, q_{v*}] and max[0, $q_t - q_{v*}$], respectively;
(iii) an air parcel conserves its total entropy;
(iv) the wave motions are in hydrostatic balance;
(v) the wave motions follow linearized equations;
(vi) the basic-state vortex has no secondary circulation;

Boundary layer drag and eddy viscosity were also ignored. Clearly, this model was not designed to precisely simulate atmospheric vortices. Rather, it was designed as a tool to easily explore the most basic effects of cloud coverage on vortex wave dynamics.

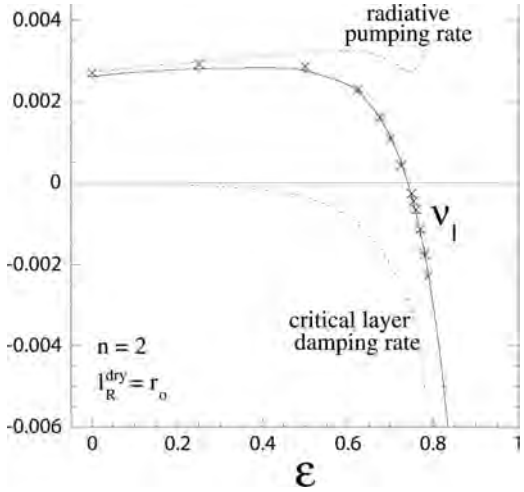

FIG. 12. Verification of the analytical growth rate formula for a discrete VR wave in a barotropic tanh cyclone, with Ro = 4. The + symbols correspond to numerical solutions of the eigenmode/quasimode problem, and the × symbols correspond to Eq. (73). The dashed curves show the radiative pumping rate ($\nu_{\rm rad}$) and critical layer damping rate ($-\nu_{\rm cl}$). Increasing cloudiness near the radius of maximum wind (increasing ε) ultimately enables critical layer damping to prevail.

The moist wave equations that result from (i)–(vi) are identical to the linearized dry hydrostatic primitive equations, with reduced cooling/warming by updrafts/downdrafts. We note that a similar model was recently reported to have been used to numerically simulate the effect of moisture on vortices that are exposed to sustained vertical shear (Patra 2004). Here, we derived the model from "first principles," in order to clarify the underlying assumptions. In addition, we provided an explicit formula for estimating the r–p variation of the buoyancy reduction factor Υ from observations [Eq. (32)].

The latter sections of this paper briefly examined the influence of moisture on eyewall instability, spontaneous IG wave radiation and vortex resilience. We have by no means closed the book on these subjects. Rather, we have presented a few case studies to motivate future research. In one case study, we showed that cloud coverage can temper the asymmetric eyewall instability of a hurricane-like vortex. In another case study, we showed that clouds in the core of a monotonic cyclone can cause or accelerate the decay of discrete VR waves. This both inhibits the spontaneous radiation of IG waves and improves vortex resilience.

Acknowledgments. The authors thank Prof. David S. Nolan and an anonymous referee for helpful reviews of this manuscript. This, work was supported by NSF Grants ATM-0528816, ATM-0132006, ATM-0349980, and ATM-0101781, and ONR Grant N00014-02-1-0474.

APPENDIX A

Thermodynamic Formulas

In this appendix, we derive convenient formulas for the moist adiabatic pressure derivatives of density potential temperature.

a. Unsaturated air

For unsaturated air, in which $q_v = q_t$, we may write

$$\theta_\rho^u = T^u\left(\frac{p_o}{p}\right)^{R_d/c_{pd}} \frac{1 + q_t/\epsilon}{1 + q_t}, \tag{A1}$$

in which $T^u(p, s_m, q_t) \equiv T(p, s_m, q_v \to q_t, q_t)$. It follows that

$$\left(\frac{\partial \theta_\rho^u}{\partial p}\right)_{s_m,q_t} = -\theta_\rho^u\left[\frac{R_d}{c_{pd}p} - \frac{1}{T^u}\left(\frac{\partial T^u}{\partial p}\right)_{s_m,q_t}\right]. \tag{A2}$$

We must now evaluate the pressure derivative of T^u at constant s_m and q_t.

To readily exploit a published result, we introduce the variable $z(p, s_m, q_t)$, defined such that

$$\left(\frac{\partial z}{\partial p}\right)_{s_m,q_t} \equiv -\frac{1}{g\rho}. \tag{A3}$$

Using Eq. (A3), we may write

$$\begin{aligned}\frac{1}{T^u}\left(\frac{\partial T^u}{\partial p}\right)_{s_m,q_t} &= -\frac{1}{g\rho T^u}\left(\frac{\partial T^u}{\partial z}\right)_{s_m,q_t} \\ &= -\frac{R_d}{gp}\frac{1 + q_t/\epsilon}{1 + q_t}\left(\frac{\partial T^u}{\partial z}\right)_{s_m,q_t}.\end{aligned} \tag{A4}$$

The above z derivative of T^u is minus the adiabatic lapse rate of an unsaturated hydrostatic atmosphere, with constant q_t. Standard texts [e.g., Emanuel 1994, Eq. (4.7.4)] derive the following formula for this lapse rate:

$$-\left(\frac{\partial T^u}{\partial z}\right)_{s_m,q_t} = \frac{g}{c_{pd}}\frac{1 + q_t}{1 + q_t c_{pv}/c_{pd}}. \tag{A5}$$

One may now execute the following chain of substitutions:

(i) substitute Eq. (A5) into Eq. (A4);
(ii) substitute Eq. (A4)′ into Eq. (A2);
(iii) substitute Eq. (A1) into Eq. (A2)′.

Here, primes indicate modified equations. The last substitution (iii) yields formula (15) of the main text.

b. Saturated air

For saturated air, in which $q_v = q_{v*}(p, s_m, q_t)$, we may write

$$\theta_\rho^s = T^s\left(\frac{p_0}{p}\right)^{R_d/c_{pd}} \frac{1 + q_{v*}/\epsilon}{1 + q_t}, \tag{A6}$$

in which $T^s(p, s_m, q_t) \equiv T(p, s_m, q_v \to q_{v*}, q_t)$. It follows that

$$\left(\frac{\partial \theta_\rho^s}{\partial p}\right)_{s_m,q_t} = -\theta_\rho^s\left[\frac{R_d}{c_{pd}p} - \frac{1}{T^s}\left(\frac{\partial T^s}{\partial p}\right)_{s_m,q_t} - \frac{1}{\epsilon + q_{v*}}\left(\frac{\partial q_{v*}}{\partial p}\right)_{s_m,q_t}\right]. \tag{A7}$$

We must now evaluate the pressure derivatives of T^s and q_{v*} at constant s_m and q_t.

To begin with, we note that

$$\frac{1}{T^s}\left(\frac{\partial T^s}{\partial p}\right)_{s_m,q_t} = -\frac{1}{g\rho T^s}\left(\frac{\partial T^s}{\partial z}\right)_{s_m,q_t} = -\frac{R_d}{gp}\frac{1 + q_{v*}/\epsilon}{1 + q_t}\left(\frac{\partial T^s}{\partial z}\right)_{s_m,q_t}, \tag{A8}$$

in which z is defined by Eq. (A3), and

$$-\left(\frac{\partial T^s}{\partial z}\right)_{s_m,q_t} = \frac{g}{c_{pd}}\frac{1 + q_t}{1 + q_{v*}c_{pv}/c_{pd}}\left[\frac{1 + L_v q_{v*}/R_d T^s}{1 + \dfrac{\mu c_l}{c_{pd} + q_{v*}c_{pv}} + \dfrac{L_v^2 q_{v*}(1 + q_{v*}/\epsilon)}{R_v (T^s)^2 (c_{pd} + q_{v*}c_{pv})}}\right]. \tag{A9}$$

The above formula for the adiabatic lapse rate of a saturated hydrostatic atmosphere is derived in Emanuel [1994, Eq. (4.7.3)].

Next, we observe that

$$q_{v*} = \epsilon\frac{e_*}{p - e_*}, \tag{A10}$$

in which e_* is the saturation vapor pressure. Since, to an excellent approximation, e_* is a function of temperature T^s alone, q_{v*} is a function of only p and T^s. Accordingly, we may write

$$\left(\frac{\partial q_{v*}}{\partial p}\right)_{s_m,q_t} = \left(\frac{\partial q_{v*}}{\partial p}\right)_{T^s} + \left(\frac{\partial q_{v*}}{\partial T^s}\right)_p\left(\frac{\partial T^s}{\partial p}\right)_{s_m,q_t} = \left(\frac{\partial q_{v*}}{\partial p}\right)_{T^s} - \frac{1}{\rho g}\left(\frac{\partial q_{v*}}{\partial T^s}\right)_p\left(\frac{\partial T^s}{\partial z}\right)_{s_m,q_t}. \tag{A11}$$

Upon differentiating Eq. (A10) with respect to p, we obtain

$$\left(\frac{\partial q_{v*}}{\partial p}\right)_{T^s} = -\frac{q_{v*}(1 + q_{v*}/\epsilon)}{p}. \tag{A12}$$

Upon differentiating Eq. (A10) with respect to T^s, and using the Clausius–Clapeyron equation,

$$\frac{de_*}{dT^s} = \frac{L_v e_*}{R_v (T^s)^2}, \tag{A13}$$

we further obtain

$$\left(\frac{\partial q_{v*}}{\partial T^s}\right)_p = \frac{L_v q_{v*}(1 + q_{v*}/\epsilon)}{R_v (T^s)^2}. \tag{A14}$$

One may now execute the following chain of substitutions:

(i) substitute Eqs. (A12) and (A14) into Eq. (A11);
(ii) substitute Eq. (A9) into Eqs. (A8) and (A11)′;
(iii) substitute Eqs. (A8)′ and (A11)″ into Eq. (A7);
(iv) substitute Eq. (A6) into Eq. (A7)′.

Here, single or double primes indicate equations that have been modified once or twice, respectively. Simplifying Eq. (A7)″ yields formula (16) of the main text.

APPENDIX B

Symmetric Stability

In the local axisymmetric model [Eqs. (35) and (36)], the perturbation equations (section 4b) have constant coefficients. Accordingly, a general disturbance is a superposition of Fourier modes, which have the form $ae^{-i(\nu t - k_p p - k_r r)}$, in which a is a complex constant. The dispersion relation is

$$\nu^2 = -\kappa^2\Upsilon\frac{\partial \overline{\theta}_\rho}{\partial p}\frac{R_d}{p}\left(\frac{p}{p_0}\right)^{R_d/c_{pd}} - 2\kappa\frac{\partial \overline{v}}{\partial p}\overline{\xi} + \overline{\eta}\,\overline{\xi}, \tag{B1}$$

in which $\kappa \equiv k_r/k_p$. Derivation of Eq. (B1) employs the thermal wind relation [Eq. (28)].

The vortex is locally stable only if $\nu^2 \geq 0$ for all κ. Considering the limits $|\kappa| \to \infty$ and $|\kappa| \to 0$, we obtain the familiar conditions of gravitational and inertial stability:

$$\Upsilon \frac{\partial \overline{\theta}_\rho}{\partial p} \leq 0 \quad \text{and} \quad \overline{\eta}\,\overline{\xi} \geq 0\,. \tag{B2}$$

Assuming gravitational stability, ν^2 is minimized when

$$\kappa = -\frac{\overline{\xi}\partial\overline{v}/\partial p}{\Upsilon\partial\overline{\theta}/\partial p}\frac{p}{R_d}\left(\frac{p_0}{p}\right)^{R_d/c_{pd}}. \tag{B3}$$

Substituting Eq. (B3) into Eq. (Bl) yields

$$\nu^2_{\min} = \frac{(\overline{\xi}\partial\overline{v}/\partial p)^2}{\Upsilon\partial\overline{\theta}_\rho/\partial p}\frac{p}{R_d}\left(\frac{p_0}{p}\right)^{R_d/c_{pd}} + \overline{\eta}\,\overline{\xi}. \tag{B4}$$

Requiring that $\nu^2_{\min} \geq 0$ gives the condition of slantwise convective stability; that is, Eq. (37) of the main text.

APPENDIX C

Numerical Simulation

In this appendix, we briefly describe the numerical model that is used to integrate the linearized wave equations (29)–(34) forward in time.

a. Prognostic equations

To begin with, let us expand each perturbation field in an azimuthal Fourier series, Specifically, let

$$\phi' = \phi_0(r, p, t) + \sum_{n=1}^{\infty}[\phi_n(r, p, t)e^{in\varphi} + \text{c.c.}], \tag{C1}$$

and likewise for all other fields. Our numerical model is based on the following prognostic equations for the Fourier coefficients:

$$\left(\frac{\partial}{\partial t} + in\overline{\Omega} + \beta\right)u_n = \overline{\xi}v_n - \frac{\partial\phi_n}{\partial r}\,, \tag{C2}$$

$$\left(\frac{\partial}{\partial t} + in\overline{\Omega} + \beta\right)v_n = -\overline{\eta}u_n - \omega_n\frac{\partial\overline{v}}{\partial p} - \frac{in}{r}\phi_n, \tag{C3}$$

and

$$\left(\frac{\partial}{\partial t} + in\overline{\Omega} + \beta\right)\theta_{\rho,n} = -u_n\frac{\partial\overline{\theta}_\rho}{\partial r} - \omega_n\Upsilon\frac{\partial\overline{\theta}_\rho}{\partial p}\,. \tag{C4}$$

Note that we have added a sponge, with Rayleigh damping coefficient $\beta(r, p)$, to absorb inertia–gravity wave radiation at the top and outer radius of the simulation domain. The damping coefficient takes the form

$$\beta \equiv \frac{\beta_s}{2}\left\{\left[1 + \tanh\left(\frac{r - r_s}{\delta r_s}\right)\right] + \left[1 + \tanh\left(\frac{p_s - p}{\delta p_s}\right)\right]\right\}, \tag{C5}$$

in which β_s, r_s, δr_s, p_s, and δp_s are adjustable constants. The simulation domain is $p_{\min} \leq p \leq p_{\max}$ and $0 < r \leq r_b$.

b. Diagnostic equations

At each time step, we must solve two diagnostic equations in order to evaluate the right-hand sides of Eqs. (C2)–(C4). The first,

$$\phi_n = \phi_n(r, p_{\min}, t) + \Im_n(r, p, t), \tag{C6}$$

is derived from hydrostatic balance. It involves the following weighted pressure integral of the density potential temperature perturbation:

$$\Im_n = -\int_{p_{\min}}^{p} d\tilde{p}\,\frac{R_d}{\tilde{p}}\left(\frac{\tilde{p}}{p_o}\right)^{R_d/c_{pd}}\theta_{\rho,n}. \tag{C7}$$

The second,

$$\omega_n = \omega_n(r, p_{\min}, t) + \mathcal{J}_n(r, p, t), \tag{C8}$$

is derived from mass continuity. It involves another pressure integral,

$$\mathcal{J}_n \equiv -\int_{p_{\min}}^{p} d\tilde{p}\left[\frac{1}{r}\frac{\partial(ru_n)}{\partial r} + \frac{in}{r}v_n\right]. \tag{C9}$$

Clearly, the right-hand sides of Eqs. (C6) and (C8) also depend on the vertical boundary conditions.

For simplicity, we here let

$$\omega_n(r, p_{\min}, t) = 0, \tag{C10}$$

and

$$\omega_n(r, p_{\max}, t) = 0. \tag{C11}$$

Constraint (C10) leaves only $\mathcal{J}_n$ on the right-hand side of Eq. (C8). Since constraint (C11) must hold at all times, we require that $\mathcal{J}_n$ at $p_{\max}$ is initially zero, and that

$$\int_{p_{\min}}^{p_{\max}} dp\,\frac{\partial}{\partial t}\left[\frac{1}{r}\frac{\partial(ru_n)}{\partial r} + \frac{in}{r}v_n\right] = 0. \tag{C12}$$

We may use the linearized velocity equations, (C2) and (C3), to evaluate the time derivative that appears in the integrand. Upon doing so, we obtain

$$\nabla_n^2\phi_n(r, p_{\min}, t) = -\int_{p_{\min}}^{p_{\max}} dp\,\frac{\mathcal{S} + \nabla_n^2\Im_n}{p_{\max} - p_{\min}}\,, \tag{C13}$$

in which

$$\nabla_n^2 \equiv \frac{1}{r}\frac{\partial}{\partial r}r\frac{\partial}{\partial r} - \frac{n^2}{r^2}\,, \tag{C14}$$

and

$$\mathcal{S} \equiv \frac{i}{r}\frac{\partial}{\partial r}[r(n\overline{\Omega} - i\beta)u_n] + \frac{in\overline{\eta}}{r}u_n - \frac{n}{r}(n\overline{\Omega} - i\beta)v_n - \frac{1}{r}\frac{\partial}{\partial r}(r\overline{\xi}v_n) + \frac{in}{r}\frac{\partial\overline{v}}{\partial p}\omega_n. \quad \text{(C15)}$$

Equation (C13) is a second-order ordinary differential equation in r for the function $\phi_n(r, p_{\min}, t)$. To solve it, we must specify boundary conditions at $r = 0$ and at $r = r_b$.

c. Radial boundary conditions

At the domain radius r_b, which is far from the vortex center, we impose an artificial wall, that is, we set

$$u_n(r_b, p, t) = 0. \quad \text{(C16)}$$

The radial velocity equation (C2) automatically maintains zero radial velocity at r_b at all times if we impose the condition

$$\frac{\partial\phi_n}{\partial r}(r_b, p, t) = \overline{\xi}(r_b, p)v_n(r_b, p, t) \quad \text{(C17)}$$

on the geopotential perturbation. Hydrostatic balance further implies that

$$\frac{\partial\theta_{\rho,n}}{\partial r}(r_b, p, t) = -\frac{p}{R_d}\left(\frac{p_0}{p}\right)^{R_d/c_{pd}}\frac{\partial}{\partial p}[\overline{\xi}(r_b, p)v_n(r_b, p, t)]. \quad \text{(C18)}$$

We impose no extra condition on the tangential velocity v_n at r_b.

At the origin ($r \to 0$) we enforce the usual constraints on the Fourier components of the perturbation fields. For the scalar fields, we have

$$\phi_n, \theta_{\rho,n} \to 0 \quad \text{for} \quad n \geq 1 \quad \text{(C19)}$$

and

$$\frac{\partial\phi_0}{\partial r}, \frac{\partial\theta_{\rho,0}}{\partial r} \to 0. \quad \text{(C20)}$$

For the velocity field, we have

$$u_n, v_n \to 0 \quad \text{for} \quad n \neq 1 \quad \text{(C21)}$$

and

$$u_1 \to -iv_1. \quad \text{(C22)}$$

d. Discretization parameters

The computational grid has N_r radial grid points and N_p pressure points. The radial grid spacing is Δr, and the pressure spacing is Δp. The first radial grid point is at $r = \Delta r$ and the last is at r_b. The first pressure grid point is at $p = p_{\min}$, and the last is at $p_{\max}$. The equations are marched forward in time with a fourth-order Runge–Kutta scheme, in steps of length Δt.

The parameters of the "hurricane" simulations of section 6 are listed below:

$$N_r = 400;\ \Delta r = 500\ \text{m};$$
$$N_p = 397;\ \Delta p = 230.66\ \text{Pa};$$
$$r_b = 200\ \text{km};$$
$$p_{\min} = 6115.12\ \text{Pa};\ p_{\max} = 97\,457.47\ \text{Pa};$$
$$r_s = 175\ \text{km};\ \delta r_s = 5\ \text{km};$$
$$p_s = 15\,000\ \text{Pa};\ \delta p_s = 2500\ \text{Pa};$$
$$\beta_s = 0.03\ \text{s}^{-1};\ \Delta t = 2.5\ \text{s}.$$

Further details of the discretization are too lengthy for discussion. Suffice it to say that the results of section 6 appear to be converged with respect to increasing spatial and temporal resolutions. In addition, the results have no appreciable change upon bringing β_s to zero.

The numerical algorithm has passed a series of tests, in which simulated eigenmodes and quasimodes were shown to behave properly. Specifically, their complex frequencies matched those obtained from the shooting method.

APPENDIX D

Asymptotic Wavefunctions

In this appendix, we present the asymptotic (small and large r) solutions of the geopotential wavefunction of an eigenmode of a barotropic vortex that has a separable Υ distribution. By assumption, the modal oscillation frequency (ν_R) is positive.

Near the origin, the only regular solution of the geopotential wavefunction is

$$\Phi_\lambda \propto r^n, \quad r \to 0. \quad \text{(D1)}$$

Recall that n is the azimuthal wavenumber.

As r becomes infinite, there are two possibilities. Let

$$k^2 \equiv \frac{\nu^2/f^2 - 1}{l_R^2(\infty)}. \quad \text{(D2)}$$

If $\Re[k^2] > 0$, then the modal oscillation can resonate with an environmental IG wave. Consequently, the mode is radiative, and

$$\Phi_\lambda \propto H_0^{(1)}(y), \quad r \to \infty. \quad \text{(D3)}$$

Here, $y = kr$, $-\pi/2 < \arg(y) \leq \pi/2$, and $H_0^{(1)}$ is a Hankel function of the first kind.

If $\Re[k^2] < 0$, then the mode is presumably evanescent. Consequently,

$$\Phi_\lambda \propto K_0(y), \quad r \to \infty. \quad \text{(D4)}$$

Here, $y = \sqrt{-k^2}r$, $-\pi/2 < \arg(y) \leq \pi/2$, and K_0 is a modified Bessel function. Note that the n dependence of the radial eigenfunction is subdominant at large radii, and appears in neither (D3) nor (D4).

APPENDIX E

Polarization Equations for an Eigenmode of a Cloudy Barotropic Vortex with Separable Υ

Solving the eigenmode problem of section 7b yields a geopotential wavefunction of the form $\Phi = \Phi_\lambda(r)\Psi_\lambda(p)$. The wavefunctions for the radial and azimuthal velocities are given by

$$U(r,p) = -\frac{i}{\overline{\psi}}\left(\sigma\frac{d\Phi_\lambda}{dr} - \frac{n\overline{\xi}}{r}\Phi_\lambda\right)\Psi_\lambda \tag{E1}$$

and

$$V(r,p) = \frac{1}{\overline{\psi}}\left(\frac{n\sigma}{r}\Phi_\lambda - \overline{\eta}\frac{d\Phi_\lambda}{dr}\right)\Psi_\lambda. \tag{E2}$$

The density potential temperature wavefunction is

$$\Theta(r,p) = -\frac{p}{R_d}\left(\frac{p_0}{p}\right)^{R_d/c_{pd}}\Phi_\lambda\frac{d\Psi_\lambda}{dp}. \tag{E3}$$

In addition to the principal polarization equations (E1)–(E3), there are several auxiliary relations. The pressure (vertical) velocity wavefunction is given by

$$W(r,p) = i\frac{\sigma}{\mathcal{RP}}\Theta, \tag{E4}$$

and the PV wavefunction by

$$\hat{\Pi}(r,p) = -\left[\frac{1}{r}\frac{\partial(rV)}{\partial r} - \frac{in}{r}U\right]\frac{d\overline{\theta}_\rho}{dp} - \overline{\eta}\frac{\partial\Theta}{\partial p}. \tag{E5}$$

Here, we have placed an aberrant circumflex over the wavefunction to prevent confusion with our symbol for total PV, $\Pi(r, \varphi, p, t)$. Finally, the wavefunction of the pseudo PV perturbation, defined in appendix F, is

$$\hat{\Pi}_p(r,p) = \frac{i}{\sigma}\frac{d\overline{\eta}}{dr}U. \tag{E6}$$

APPENDIX F

Wave Activity in a Cloudy Barotropic Vortex

Our construction of a wave activity principle requires that we first introduce a pseudo potential vorticity perturbation,

$$\Pi'_p \equiv \left[\Pi' + \eta'_z\overline{\chi} + \theta'_\rho\overline{\eta}\frac{\partial}{\partial p}\ln\left(\Upsilon\frac{d\overline{\theta}_\rho}{dp}\right)\right]\left(\Upsilon\frac{d\overline{\theta}_\rho}{dp}\right)^{-1}$$
$$= -\overline{\eta}\frac{\partial}{\partial p}\left(\frac{\theta'_\rho}{\Upsilon d\overline{\theta}_\rho/dp}\right) - \eta'_z, \tag{F1}$$

in which

$$\eta'_z \equiv \hat{\mathbf{z}}\cdot\boldsymbol{\eta}' = \frac{1}{r}\frac{\partial(rv')}{\partial r} - \frac{1}{r}\frac{\partial u'}{\partial\varphi}. \tag{F2}$$

For a barotropic vortex, one can readily verify that

$$\left(\frac{\partial}{\partial t} + \overline{\Omega}\frac{\partial}{\partial\varphi}\right)\Pi'_p = u'\frac{d\overline{\eta}}{dr}, \tag{F3}$$

in the context of linear theory.

A convenient local measure of wave activity is the moist angular pseudomomentum,

$$\mathcal{L}_p \equiv -\frac{r(\Pi'_p)^2}{2d\overline{\eta}/dr} - \frac{r}{\Upsilon d\overline{\theta}_\rho/dp}\theta'_\rho\frac{\partial v'}{\partial p}. \tag{F4}$$

The moist angular pseudomomentum satisfies the flux conservative equation,

$$\frac{\partial\mathcal{L}_p}{\partial t} + \boldsymbol{\nabla}\cdot\boldsymbol{\mathcal{F}}_p = 0, \tag{F5}$$

in which

$$\boldsymbol{\mathcal{F}}_p \equiv -ru'v'\hat{\mathbf{r}} + \left\{\overline{v}\mathcal{L}_p + r\left[\frac{(u')^2}{2} - \frac{(v')^2}{2}\right] + r\left(\frac{p}{p_0}\right)^{R_d/c_{pd}}\frac{R_d(\theta'_\rho)^2}{2p\Upsilon d\overline{\theta}_\rho/dp}\right\}\hat{\boldsymbol{\varphi}}$$
$$+ \left(\frac{r\overline{\eta}}{\Upsilon d\overline{\theta}_\rho/dp}u'\theta'_\rho + rv'\omega'\right)\hat{\mathbf{z}}. \tag{F6}$$

The reader may verify Eq. (F5) in a straightforward manner, using Eqs. (30), (31), (33), (62), and (F3).

Integrating Eq. (F5) over a cylinder of radius r_v, bounded above and below at $p_{\min}$ and $p_{\max}$, yields

$$\frac{dA}{dt} = \int_{p_{\min}}^{p_{\max}}\int_{-\pi}^{\pi}dp\,d\varphi[r^2u'v']_{r_v} + \int_0^{r_v}\int_{-\pi}^{\pi}dr\,d\varphi\left[\frac{r^2\overline{\eta}}{\Upsilon d\overline{\theta}_\rho/dp}u'\theta'_\rho + r^2v'\omega'\right]_{p_{\min}}^{p_{\max}}, \tag{F7}$$

in which

$$A \equiv \int_{p_{\min}}^{p_{\max}}\int_0^{r_v}\int_{-\pi}^{\pi}dp\,dr\,d\varphi r\mathcal{L}_p \tag{F8}$$

is the total wave activity in the cylinder. The total wave activity equation (F7) is crucial for deriving the growth rate formula [Eq. (73)] of a discrete VR wave in a barotropic vortex, following the procedure of Schecter and Montgomery (2004, 2006).

Suppose that $\theta'_\rho = 0$ at $p_{\min}$ and $p_{\max}$. Then, by the linearized heat equation (31) of a barotropic vortex, ω' would also be zero on the vertical boundaries. As such, the second (radial) integral on the right-hand side of Eq. (F7) would vanish.

APPENDIX G

The Meaning of Υ

In this appendix, we clarify the motivation for calling Υ the "buoyancy reduction factor." This nomenclature alludes to the reduction of the vertical ($\hat{\mathbf{z}}$) buoyancy restoring force that a parcel feels after a moist adiabatic vertical displacement, or pressure change (cf. Smith et al. 2005). The vertical buoyancy acceleration is defined by

$$B \equiv -g\frac{\rho'}{\overline{\rho}}, \tag{G1}$$

in which ρ' is the local perturbation from the basic-state density

$$\overline{\rho} \equiv \frac{p}{\overline{\theta}_\rho R_d}\left(\frac{p_o}{p}\right)^{R_d/c_{pd}}. \tag{G2}$$

Consider a moist fluid parcel that moves from the pressure level $p - \delta p$ to p. We may write the density change of the parcel as follows:

$$\begin{aligned}\delta\rho &= \left(\frac{\partial\rho}{\partial p}\right)_{\theta_\rho}\delta p + \left(\frac{\partial\rho}{\partial\theta_\rho}\right)_{p}\delta\theta_\rho \\ &= \frac{c_{vd}\rho}{c_{pd}p}\delta p - \frac{\rho}{\theta_\rho}\delta\theta_\rho,\end{aligned} \tag{G3}$$

in which the new symbol c_{vd} is the specific heat of dry air at constant volume, and the coefficients of the infinitesimals are evaluated at the original parcel position.

Assume that the parcel initially has basic-state values of density and density potential temperature. Further assume that the parcel keeps its radial coordinate r fixed. Then, the density perturbation at the new parcel position is given by

$$\begin{aligned}\rho' &= \overline{\rho}(r, p - \delta p) + \delta\rho - \overline{\rho}(r, p) \\ &= \left(\frac{c_{vd}\overline{\rho}}{c_{pd}p} - \frac{\partial\overline{\rho}}{\partial p}\right)\delta p - \frac{\overline{\rho}}{\overline{\theta}_\rho}\delta\theta_\rho.\end{aligned} \tag{G4}$$

It is straightforward to show that

$$\frac{c_{vd}\overline{\rho}}{c_{pd}p} - \frac{\partial\overline{\rho}}{\partial p} = \frac{\partial\overline{\theta}_\rho}{\partial p}\frac{\overline{\rho}}{\overline{\theta}_\rho}. \tag{G5}$$

Furthermore, by way of Eq. (14) we may write

$$\delta\theta_\rho = \chi\delta p, \tag{G6}$$

in which χ is evaluated at the original parcel position.

Substituting Eqs. (G5) and (G6) into (G4), and then Eq. (G4) into (Gl) leads to the following expression for the vertical buoyancy acceleration at the new parcel position:

$$B = -\frac{g}{\overline{\theta}_\rho}\frac{\partial\overline{\theta}_\rho}{\partial p}\Upsilon_{\mathrm{prcl}}\delta p, \tag{G7}$$

in which

$$\Upsilon_{\mathrm{prcl}} \equiv \frac{\partial\overline{\theta}_\rho/\partial p - \chi}{\partial\overline{\theta}_\rho/\partial p}. \tag{G8}$$

Assuming that the vortex is gravitationally stable, Υ_{prcl} is between zero and one; therefore, it generally reduces the magnitude of B. Υ, defined in the main text, is a tempero-azimuthal mean of Υ_{prcl}.

REFERENCES

Abramowitz, M., and A. Stegun, 1972: *Handbook of Mathematical Functions.* Dover, 1046 pp.

Balmforth, N. J., S. G. Llewellyn Smith, and W. R. Young, 2001: Disturbing vortices. *J. Fluid Mech.,* **426,** 95–133.

Bassom, A. P., and A. D. Gilbert, 1998: The spiral wind-up of vorticity in an inviscid planar vortex. *J. Fluid Mech.,* **371,** 109–140.

Briggs, R. J., J. D. Daugherty, and R. H. Levy, 1970: Role of Landau damping in crossed-field electron beams and inviscid shear flow. *Phys. Fluids,* **13,** 421–432.

Chen, Y., and M. K. Yau, 2001: Spiral bands in a simulated hurricane. Part I: Vortex Rossby wave verification. *J. Atmos. Sci.,* **58,** 2128–2145.

——, G. Brunet, and M. K. Yau, 2003: Spiral bands in a simulated hurricane. Part II: Wave activity diagnostics. *J. Atmos. Sci.,* **60,** 1239–1256.

Chow, K. C., and K. L. Chan, 2003: Angular momentum transports by moving spiral waves. *J. Atmos. Sci.,* **60,** 2004–2009.

——, ——, and A. K. H. Lau, 2002: Generation of moving spiral bands in tropical cyclones. *J. Atmos. Sci.,* **59,** 2930–2950.

Cotton, W. R., and Coauthors, 2003: RAMS 2001: Current status and future directions. *Meteor. Atmos. Phys.,* **82,** 5–29.

Davidson, R. C., 1990: *Physics of Nonneutral Plasmas.* Addison-Wesley, 733 pp.

Dunkerton, T. J., 1990: Eigenfrequencies and horizontal structure of divergent barotropic instability originating in tropical latitudes. *J. Atmos. Sci.,* **47,** 1288–1301.

Durran, D. R., and J. P. Klemp, 1982: On the effects of moisture on the Brunt–Väisälä frequency. *J. Atmos. Sci.,* **39,** 2152–2158.

Emanuel, K. A., 1986: An air–sea interaction theory for tropical cyclones. Part I: Steady state maintenance. *J. Atmos. Sci.,* **43,** 585–604.

——, 1994: *Atmospheric Convection.* Oxford University Press, 580 pp.

——, 1997: Some aspects of hurricane inner-core dynamics and energetics. *J. Atmos. Sci.,* **54,** 1014–1026.

Enagonio, J., and M. T. Montgomery, 2001: Tropical cyclogenesis via convectively forced Rossby waves in a shallow-water primitive equation model. *J. Atmos. Sci.,* **58,** 685–706.

Ford, R., 1994a: The instability of an axisymmetric vortex with monotonic potential vorticity in rotating shallow water. *J. Fluid Mech.,* **280,** 303–334.

——, 1994b: The response of a rotating ellipse of uniform potential vorticity to gravity wave radiation. *Phys. Fluids,* **6,** 3694–3704.

Gall, R. L., 1983: A linear analysis of multiple vortex phenomenon in simulated tornadoes. *J. Atmos. Sci.,* **40,** 2010–2024.

Jones, S. C., 1995: The evolution of vortices in vertical shear. I. Initially barotropic vortices. *Quart. J. Roy. Meteor. Soc.,* **121,** 821–851.

Jordan, C. L., 1958: Mean soundings for the West Indies area. *J. Meteor.,* **15,** 91–97.

Kelvin, L., 1880: On the vibrations of a columnar vortex. *Phil. Mag.,* **10,** 155–168.

Kossin, J. P., and W. H. Schubert, 2001: Mesovortices, polygonal flow patterns, and rapid pressure falls in hurricane-like vortices. *J. Atmos. Sci.,* **58,** 2196–2209.

Mallen, K. J., M. T. Montgomery, and B. Wang, 2005: Reexamining the near-core radial structure of the tropical cyclone primary circulation: Implications for vortex resiliency. *J. Atmos. Sci.,* **62,** 408–425.

McWilliams, J. C., L. P. Graves, and M. T. Montgomery, 2003: A formal theory for vortex Rossby waves and vortex evolution. *Geophys. Astrophys. Fluid Dyn.,* **97,** 275–309.

Michalke, A., and A. Timme, 1967: On the inviscid instability of certain two-dimensional vortex-type flows. *J. Fluid Mech.,* **29,** 647–666.

Möller, J. D., and M. T. Montgomery, 1999: Vortex Rossby waves and hurricane intensification in a barotropic model. *J. Atmos. Sci.,* **56,** 1674–1687.

——, and ——, 2000: Tropical cyclone evolution via potential vorticity anomalies in a three-dimensional balance model. *J. Atmos. Sci.,* **57,** 3366–3387.

Montgomery, M. T., and L. J. Shapiro, 1995: Generalized Charney–Stern and Fjortoft theorems for rapidly rotating vortices. *J. Atmos. Sci.,* **52,** 1829–1833.

——, and R. J. Kallenbach, 1997: A theory of vortex Rossby-waves and its application to spiral bands and intensity changes in hurricanes. *Quart. J. Roy. Meteor. Soc.,* **123,** 435–465.

——, and J. Enagonio, 1998: Tropical cyclogenesis via convectively forced vortex Rossby waves in a three-dimensional quasigeostrophic model. *J. Atmos. Sci.,* **55,** 3176–3207.

——, and J. L. Franklin, 1998: An assessment of the balance approximation in hurricanes. *J. Atmos. Sci.,* **55,** 2193–2200.

——, V. A. Vladimirov, and P. V. Denissenko, 2002: An experimental study on hurricane mesovortices. *J. Fluid Mech.,* **471,** 1–32.

——, M. Bell, S. D. Aberson, and M. Black, 2006: Hurricane Isabel (2003): New insights into the physics of intense storms. Part I: Mean vortex structure and maximum intensity estimates. *Bull. Amer. Meteor. Soc.,* **87,** 1335–1347.

Nolan, D. S., and M. T. Montgomery, 2002: Nonhydrostatic, three-dimensional perturbations to balanced, hurricane-like vortices. Part I: Linearized formulation, stability, and evolution. *J. Atmos. Sci.,* **59,** 2989–3020.

Ooyama, K., 1966: On the stability of the baroclinic circular vortex. *J. Atmos. Sci.,* **23,** 43–53.

Patra, R., 2004: Idealized modeling of tropical cyclones in vertical shear: The role of saturated ascent in the inner core. Preprints, *26th Conf. on Hurricanes and Tropical Meteorology,* Miami, FL, Amer. Meteor. Soc., 98–99.

Persing, J., and M. T. Montgomery, 2003: Hurricane superintensity. *J. Atmos. Sci.,* **60,** 2349–2371.

Pillai, S., and R. W. Gould, 1994: Damping and trapping in 2D inviscid fluids. *Phys. Rev. Lett.,* **73,** 2849–2852.

Plougonven, R., and V. Zeitlin, 2002: Internal gravity wave emission from a pancake vortex: An example of wave-vortex interaction in strongly stratified flows. *Phys. Fluids,* **14,** 1259–1268.

Polvani, L. M., J. C. McWilliams, M. A. Spall, and R. Ford, 1994: The coherent structures of shallow-water turbulence: Deformation-radius effects, cyclone/anticyclone asymmetry and gravity-wave generation. *Chaos,* **4,** 177–186.

Reasor, P. D., and M. T. Montgomery, 2001: Three-dimensional alignment and co-rotation of weak, TC-like vortices, via linear vortex Rossby waves. *J. Atmos. Sci.,* **58,** 2306–2330.

——, ——, and L. D. Grasso, 2004: A new look at the problem of tropical cyclones in shear flow: Vortex resiliency. *J. Atmos. Sci.,* **61,** 3–22.

Ren, S., 1999: Further results on the stability of rapidly rotating vortices in the asymmetrical balance formation. *J. Atmos. Sci.,* **56,** 475–482.

Rotunno, R., 1978: A note on the stability of a cylindrical vortex sheet. *J. Fluid Mech.,* **87,** 761–771.

Schecter, D. A., and M. T. Montgomery, 2003: On the symmetrization rate of an intense geophysical vortex. *Dyn. Atmos. Oceans,* **37,** 55–87.

——, and ——, 2004: Damping and pumping of a vortex Rossby wave in a monotonic cyclone: Critical layer stirring versus inertia-buoyancy wave emission. *Phys. Fluids,* **16,** 1334–1348.

——, and ——, 2006: Conditions that inhibit the spontaneous radiation of spiral inertia–gravity waves from an intense mesoscale cyclone. *J. Atmos. Sci.,* **63,** 435–456.

——, D. H. E. Dubin, A. C. Cass, C. F. Driscoll, I. M. Lansky, and T. M. O'Neil, 2000: Inviscid damping of asymmetries on a two-dimensional vortex. *Phys. Fluids,* **12,** 2397–2412.

——, M. T. Montgomery, and P. D. Reasor, 2002: A theory for the vertical alignment of a quasigeostrophic vortex. *J. Atmos. Sci.,* **59,** 150–168.

Schubert, W. H., M. T. Montgomery, R. K. Taft, T. A. Guinn, S. R. Fulton, J. P. Kossin, and J. P. Edwards, 1999: Polygonal eyewalls, asymmetric eye contraction, and potential vorticity mixing in hurricanes. *J. Atmos. Sci.,* **56,** 1197–1223.

Shapiro, L. J., and M. T. Montgomery, 1993: A three-dimensional balance theory for rapidly rotating vortices. *J. Atmos. Sci.,* **50,** 3322–3335.

Smith, R. K., M. T. Montgomery, and H. Zhu, 2005: Buoyancy in tropical cyclones and other rapidly rotating atmospheric vortices. *Dyn. Atmos. Oceans,* **40,** 189–208.

Spencer, R. L., and S. N. Rasband, 1997: Damped diocotron quasi-modes of nonneutral plasmas and inviscid fluids. *Phys. Plasmas,* **4,** 53–60.

Terwey, W. D., and M. T. Montgomery, 2002: Wavenumber-2 and wavenumber-m vortex Rossby wave instabilities in a generalized three-region model. *J. Atmos. Sci.,* **59,** 2421–2427.

Vladimirov, V. A., and V. F. Tarasov, 1980: Formation of a system of vortex filaments in a rotating liquid. *Izv. Akad. Az. Nauk SSSr, Mekh. Zhid. i Gaza,* **1,** 44–51.

Wang, Y., 2002a: Vortex Rossby waves in a numerically simulated tropical cyclone. Part I: Overall structure, potential vorticity, and kinetic energy budgets. *J. Atmos. Sci.,* **59,** 1213–1238.

——, 2002b: Vortex Rossby waves in a numerically simulated tropical cyclone. Part II: The role in tropical cyclone structure and intensity changes. *J. Atmos. Sci.,* **59,** 1239–1262.

Ward, N. B., 1972: The exploration of certain features of tornado dynamics using a laboratory model. *J. Atmos. Sci.,* **29,** 1194–1204.

Weske, J. R., and T. M. Rankin, 1963: Generation of secondary motions in the fields of a vortex. *Phys. Fluids,* **6,** 1397–1403.